A calcium-sensing receptor mutation causing hypocalcemia disrupts a transmembrane salt bridge to activate β-arrestin-biased signaling

Caroline M. Gorvin[1], Valerie N. Babinsky[1], Tomas Malinauskas[2], Peter H. Nissen[3], Anders J. Schou[4], Aylin C. Hanyaloglu[5], Christian Siebold[2], E. Yvonne Jones[2], Fadil M. Hannan[1,6*], Rajesh V. Thakker[1*]

[1]Academic Endocrine Unit, Oxford Centre for Diabetes, Endocrinology and Metabolism, Radcliffe Department of Medicine, University of Oxford, Oxford, OX3 7LJ, UK

[2]Division of Structural Biology, Wellcome Trust Centre for Human Genetics, University of Oxford, Oxford, OX3 7BN, UK

[3]Department of Clinical Biochemistry, Aarhus University Hospital, DK-8200 Aarhus N, Denmark

[4]Hans Christian Andersen Children's Hospital, Odense University Hospital, 5000 Odense C, Denmark

[5]Institute of Reproductive and Developmental Biology, Faculty of Medicine, Imperial College London, W12 0NN, UK

[6]Institute of Ageing and Chronic Disease, University of Liverpool, Liverpool, L7 8TX, UK

[*]Corresponding authors. Email: rajesh.thakker@ndm.ox.ac.uk; Fadil.Hannan@liverpool.ac.uk

One-Sentence Summary:
A genetic disease–associated mutation disrupts a calcium-sensing receptor structural motif causing biased signaling through β-arrestin.

Editor's Summary:
GPCR signaling biased by a salt bridge
The calcium-sensing receptor (CaSR) is a G protein–coupled receptor (GPCR) that plays an important role in extracellular calcium homeostasis by stimulating intracellular calcium signaling and mitogen-activated protein kinase (MAPK) pathways. Mutations in *CASR* that specifically affect either intracellular calcium or MAPK signaling have been associated with inherited forms of hypocalcemia. Gorvin *et al*. identified a *CASR* mutation that results in an Arg-to-Gly substitution at amino acid position 680 (R680G) in CaSR, in a family with hypocalcemia. Functional analysis of $CaSR^{R680G}$ in cultured cells revealed that this missense mutation did not affect intracellular calcium signaling but enhanced the ability of CaSR to stimulate MAPK through a mechanism that depended on the scaffolding protein β-arrestin, rather than on G proteins. Structural modeling and mutational analysis

demonstrated that the substitution likely disrupted a salt bridge in CaSR. These findings identify a structural feature of CaSR that is important for controlling signaling bias.

ABSTRACT

The calcium-sensing receptor (CaSR) is a G protein–coupled receptor (GPCR) that signals through $G_{q/11}$ and $G_{i/o}$ to stimulate cytosolic calcium (Ca^{2+}_i) and mitogen-activated protein kinase (MAPK) signaling to control extracellular calcium homeostasis. Studies of loss- and gain-of-function *CASR* mutations, which cause familial hypocalciuric hypercalcemia type 1 (FHH1) and autosomal dominant hypocalcemia type 1 (ADH1), respectively, have revealed the CaSR to signal in a biased manner. Thus, some mutations associated with FHH1 lead to signaling predominantly through the MAPK pathway, whereas mutations associated with ADH1 preferentially enhance Ca^{2+}_i responses. Here, we report a previously unidentified ADH1-associated R680G CaSR mutation, which led to the identification of a CaSR structural motif that mediates biased signaling. Expressing the R680G CaSR mutant in HEK293 cells showed that this mutation increased MAPK signaling without altering Ca^{2+}_i responses. Moreover, this gain-of-function in MAPK activity occurred independently of $G_{q/11}$ and $G_{i/o}$, and was mediated instead by a non-canonical pathway involving β-arrestin scaffolding proteins. Homology modeling and mutagenesis studies showed the R680G CaSR mutation selectively enhanced β-arrestin signaling by disrupting a salt bridge formed between Arg^{680} and Glu^{767}, which are located in the CaSR transmembrane domain 3 and extracellular loop-2, respectively. Thus, our results demonstrate CaSR signaling through β-arrestin and the importance of the Arg^{680}-Glu^{767} salt bridge in mediating signaling bias.

INTRODUCTION

The calcium-sensing receptor (CaSR) is a family C G protein–coupled receptor (GPCR) that is highly abundant in the parathyroid glands and kidneys and plays an essential role in extracellular calcium (Ca^{2+}_e) homeostasis by decreasing parathyroid hormone (PTH) secretion and increasing urinary calcium excretion in response to elevations in Ca^{2+}_e concentrations (*1*). The human CaSR is encoded by the *CASR* gene located on chromosome 3q21.1 and consists of: an extracellular domain, which binds Ca^{2+}_e and mediates receptor dimerization; seven transmembrane domains (TMDs); and an intracellular domain, which is involved in activation of downstream signaling effectors such as G proteins and phospholipase C (PLC) (*2, 3*). The CaSR stimulates two major signal transduction cascades. The first is the $G_{q/11}$-phospholipase C (PLC)-mediated generation of inositol 1,4,5-trisphosphate (IP_3), which induces a rapid rise in intracellular calcium (Ca^{2+}_i) concentrations (*4*). The second is the mitogen-activated protein kinases (MAPKs), such as extracellular signal–regulated kinases 1 and 2 (ERK1/2), which phosphorylate proteins mediating cytosolic signaling and translocate into the nucleus to activate transcription factors involved in cellular proliferation and differentiation (*5*). The CaSR has been shown to activate MAPK signaling in a manner that depends on the G proteins $G_{q/11}$, and $G_{i/o}$, which inhibits cyclic adenosine monophosphate (cAMP) synthesis, and by a potentially G protein–independent mechanism involving β-arrestin types 1 and 2 (*6*). β-arrestins are intracellular scaffolding proteins that play a critical role in inactivating GPCRs by inhibiting interactions with G proteins and by targeting these receptors for clathrin-mediated endocytosis (*7*). Moreover, β-arrestins have been shown to enhance GPCR-mediated MAPK signaling from clathrin-coated structures (*8*).

The importance of the CaSR in the regulation of Ca^{2+}_e has been highlighted by the identification of loss-of-function CaSR mutations that give rise to familial hypocalciuric hypercalcemia type 1 (FHH1) and neonatal severe hyperparathyroidism (NSHPT), as well as by gain-of-function CaSR mutations that cause autosomal dominant hypocalcemia type 1 (ADH1), which is characterized by hypocalcemia, hyperphosphatemia, normal or low circulating PTH concentrations, ectopic

calcifications, and a relative or absolute hypercalciuria (*9, 10*). Functional studies have demonstrated that these disease-causing mutations may influence the signaling responses of CaSR-expressing cells in a biased manner (*11*). Thus, some FHH1-causing mutations switch the CaSR from preferentially coupling to Ca^{2+}_i to signaling equally through the Ca^{2+}_i and MAPK pathways or predominantly through MAPK (*11*). In contrast, many ADH1-associated CaSR mutations lead to a signaling bias by causing CaSR to couple more strongly to Ca^{2+}_i (*11*) than to MAPK pathways. Studies involving positive and negative allosteric CaSR-modulating compounds, known as calcimimetics and calcilytics, respectively, have also revealed biased signaling responses, with both classes of drugs influencing Ca^{2+}_i to a greater extent than they do ERK1/2 phosphorylation (*12*). Although these findings have established that agonist-induced CaSR signaling may occur in a biased manner, the GPCR structural motifs that mediate ligand-dependent bias remain to be elucidated. Here, we describe a previously unidentified ADH1-causing mutation that affects the Arg^{680} residue of CaSR, which is located at the outer membrane end of TMD3. Our studies show that this residue is involved in forming a salt bridge with the extracellular loop 2 (ECL2) residue Glu^{767}. This salt bridge influences β-arrestin signaling, and its disruption leads to enhanced MAPK signaling without altering Ca^{2+}_i responses.

RESULTS

A CaSR^{R680G} mutation is responsible for autosomal dominant hypocalcemia type 1 (ADH1) in a family

The proband, a 7-year-old male, presented with hypocalcemic symptoms (Table S1). The hypocalcemia was associated with a low serum PTH concentration. His father also had hypocalcemia, whereas his mother and two paternal half-siblings were normocalcemic (Fig. 1A, Table S1). DNA sequence analysis of *CASR* in the proband and his father (Fig. 1A) identified a heterozygous C-to-G transition at nucleotide c.2038 (Fig. 1B), which resulted in a missense substitution of Arg^{680} to Gly (R680G) (Fig. 1C) that is located in TMD3 of the CaSR protein (Fig. 1D). Bioinformatic analyses using the Polyphen-2 and MutationTasting websites (*13, 14*) predicted the R680G mutation to be damaging and likely disease-causing (Polyphen-2 score 1, MutationTasting score 0.99). The absence of this DNA sequence abnormality in >6500 exomes from the National Heart, Lung and Blood Institute Exome Sequencing Project (NHLBI-ESP) cohort and >60,700 exomes from the Exome Aggregation Consortium (ExAC) cohort, together with evolutionary conservation of the Arg^{680} residue in the CaSR (Fig. 1D), also indicated that R680G likely represents a pathogenic mutation rather than a benign polymorphic variant. Furthermore, mutations involving this residue have been reported in two cases of FHH, in which Arg^{680} was mutated to either a Cys or His residue, indicating that the Arg^{680} residue is important in CaSR function (*11, 15*). We therefore characterized the effects of the R680G missense mutation in vitro to determine its effect on CaSR-mediated signaling.

CaSR^{R680G} is present at the plasma membrane and does not exhibit abnormal intracellular calcium signaling

FHH1-causing mutations at Arg^{680} have been reported to decrease CaSR accumulation at the cell surface (*11*). We therefore evaluated whether the ADH1-causing R680G mutation may also affect the abundance of CaSR at the plasma membrane. Western blot analyses, using cytoplasmic and plasma membrane fractions of HEK293 cells transiently transfected with plasmid constructs that expressed

either the wild-type ($CaSR^{WT}$) or mutant ($CaSR^{R680G}$) CaSR fused to the N-terminus of enhanced GFP (pEGFP-N1) (*16, 17*), revealed both $CaSR^{WT}$ and $CaSR^{R680G}$ to be present at the cell surface (fig. S1A-S1D). Furthermore, quantification of the abundance of $CaSR^{WT}$ and $CaSR^{R680G}$ at the plasma membrane by Western blot analyses of cells that transiently expressed each protein and were biotinylated using the membrane-impermeant sulfo-NHS-SS-biotin, revealed that the abundance of $CaSR^{WT}$ and $CaSR^{R680G}$ at the cell surface was not significantly different (fig. S1, S2A-S2C). Thus, unlike the FHH-causing mutations at Arg^{680}, the R680G mutation did not alter the abundance of the CaSR at the plasma membrane.

To assess the effects of the R680G mutation on CaSR-mediated $Ca^{2+}{}_i$ responses, we transiently transfected HEK293 cells with pEGFP-N1-CASR constructs that expressed EGFP-tagged versions of $CaSR^{WT}$, $CaSR^{R680G}$, or the previously characterized ADH1-causing L173F mutant CaSR ($CaSR^{L173F}$) (*16*). Expression of CaSRs was confirmed by Western blot analysis (Fig. 2A). The $Ca^{2+}{}_i$ responses in cells expressing wild-type or mutant CaSRs, as measured by a Fluo-4 intracellular calcium assay (*18*), increased in a dose-dependent manner in response to stimulation with increasing $Ca^{2+}{}_e$ concentrations ($[Ca^{2+}]_e$) of 0-15mM (Fig. 2, B and C), as expected. Expression of $CaSR^{L173F}$ resulted in a leftward shift of the concentration-response curve (Fig. 2B), with a significantly lower half maximal (EC_{50}) value, compared to expression of $CaSR^{WT}$ (Fig. 2, B and C), whereas the EC_{50} value for cells expressing $CaSR^{R680G}$ was not significantly different from cells expressing $CaSR^{WT}$. Thus, the EC_{50} for cells expressing $CaSR^{WT}$ was 2.64mM (95% confidence interval (CI) = 2.40-2.89mM), compared to 1.68mM (95%CI = 1.50-1.89mM) for $CaSR^{L173F}$-expressing cells, and 2.73mM (95%CI = 2.56-2.90mM) for $CaSR^{R680G}$-expressing cells (Fig. 2, B and C). Therefore, the R680G mutation did not affect $Ca^{2+}{}_i$ signaling downstream of CaSR. Previous studies have demonstrated that the Arg^{680} residue lies within the binding pocket for the calcilytic compound NPS-2143 (*18*). To investigate whether the R680G mutation may disrupt NPS-2143–mediated allosteric inhibition of the CaSR, we measured the $Ca^{2+}{}_i$ responses of cells expressing the L173F or R680G mutant forms of CaSR in the presence of 500nM NPS-2143, a concentration 25 times greater than that required to normalize a reported gain-of-function CaSR mutation (*19*). Treatment with 500nM NPS-2143 significantly

increased the EC_{50} of $CaSR^{WT}$-expressing cells to 3.81mM (95% CI = 3.56-4.08mM) compared to untreated $CaSR^{WT}$-expressing cells and that of $CaSR^{L173F}$-expressing cells to 3.34mM (95% CI = 3.12-3.57mM) compared to untreated $CaSR^{L173F}$-expressing cells (Fig. 2, B and C). In contrast, this concentration of NPS-2143 had no significant effect on the EC_{50} values of cells expressing $CaSR^{R680G}$ (Fig. 2, B and C). Thus, the R680G mutation abrogated the effect of NPS-2143 on CaSR-mediated $Ca^{2+}{}_i$ responses.

To verify the findings of the $Ca^{2+}{}_i$ Fluo-4 assays, we performed luciferase reporter assays using a construct containing a nuclear factor of activated T-cells (NFAT) response element, which is activated by increases in $Ca^{2+}{}_i$ (*20*). We measured NFAT luciferase reporter activity in HEK293 cells transiently co-transfected with the reporter construct and $CaSR^{WT}$, $CaSR^{R680G}$ or $CaSR^{L173F}$. Western blot analysis confirmed the expression of wild-type and mutant CaSRs in these cells (Fig. 2D), and the NFAT reporter activity increased in a dose-dependent manner following stimulation with increasing $[Ca^{2+}]_e$ (Fig. 2E). Cells expressing $CaSR^{L173F}$ showed significantly increased NFAT fold-change responses (fold-change = 13.8 ± 1.1 following exposure to 5mM $[Ca^{2+}]_e$), compared to cells expressing $CaSR^{WT}$ (fold-change = 6.1 ± 0.7, Fig. 2E). In contrast, $CaSR^{R680G}$-expressing cells had similar NFAT reporter activity (fold-change = 8.7 ± 1.7) to that of cells expressing $CaSR^{WT}$ (Fig. 2E).

The R680G mutation increases MAPK signaling downstream of CaSR

To assess whether the R680G CaSR mutation may influence MAPK signaling, we measured fold-changes in phosphorylated ERK1/2 in response to increasing $[Ca^{2+}]_e$ in HEK293 cells transiently expressing $CaSR^{WT}$, $CaSR^{R680G}$, or $CaSR^{L173F}$. Densitometric analysis of Western blots revealed that stimulation with 5mM $[Ca^{2+}]_e$, when compared to 0mM $[Ca^{2+}]_e$, increased ERK1/2 phosphorylation responses of cells expressing wild-type and mutant CaSRs (Fig. 3A and 3B and fig. S3A-S3D), but ERK1/2 phosphorylation was significantly greater in cells expressing the mutant forms of CaSR compared to cells expressing the wild-type CaSR. To further assess these responses, we measured accumulation of phosphorylated ERK1/2 in response to 0-10mM $[Ca^{2+}]_e$ using AlphaScreen analysis

(Fig. 3C and 3D) following Western blotting to confirm the expression of wild-type and mutant CaSRs in the cells (Fig. 3C). $Ca^{2+}{}_e$ stimulation induced a dose-dependent increase in phosphorylated ERK1/2 fold-change responses in all cells (Fig. 3D). These responses were significantly increased at 10mM $[Ca^{2+}]_e$, a concentration that has been reported to lead to near-maximal signaling responses in CaSR-expressing HEK293 cells (*21*), in both the $CaSR^{R680G}$- and $CaSR^{L173F}$-expressing cells (4.7 ± 0.1 and 5.2 ± 0.2, respectively), compared to cells expressing $CaSR^{WT}$ (3.6 ± 0.1) (Fig. 3D). We also investigated the effect of the R680G CaSR mutation on MAPK signaling by measuring gene transcription induced by a luciferase reporter construct containing a serum-response element (SRE), which is a downstream target of ERK1/2 signaling (*21, 22*). Western blot analysis confirmed expression of wild-type and mutant CaSRs in cells used for the SRE reporter experiments (Fig. 3E), and exposure to $Ca^{2+}{}_e$ led to a dose-dependent increase in SRE reporter activity in all cell types (Fig. 3F). Expression of the $CaSR^{R680G}$ or $CaSR^{L173F}$ significantly increased fold-change responses at 10mM $[Ca^{2+}]_e$ (R680G = 25 ± 4,; and L173F = 38 ± 8) compared to cells expressing $CaSR^{WT}$ (15 ± 2) (Fig. 3F). Thus, the R680G mutation increased MAPK signaling, consistent with this being a gain-of-function mutation (*11*). To determine whether the $CaSR^{R680G}$ may interfere with the effect of NPS-2143 on CaSR-induced MAPK signaling, we repeated the SRE experiment in the presence of 500nM NPS-2143 and following stimulation with 10mM $[Ca^{2+}]_e$. The presence of NPS-2143 did not alter expression of the wild-type or mutant CaSRs (Fig. 3G) or affect the SRE reporter responses of cells expressing the $CaSR^{R680G}$, but it reduced SRE reporter responses of cells expressing $CaSR^{WT}$ or $CaSR^{L173F}$ (Fig. 3H). Thus, the R680G mutation abolished the effect of NPS-2143 on CaSR-mediated MAPK signaling.

The increased MAPK responses of $CaSR^{R680G}$ occur independently of $G_{q/11}$ and $G_{i/o}$

Compared to $CaSR^{WT}$, $CaSR^{R680G}$ exhibited increased ERK1/2 phosphorylation (Fig. 3) without altered $Ca^{2+}{}_i$ responses (Fig. 2). To determine whether this biased signaling depended on G proteins, we further investigated $G_{q/11}$- and $G_{i/o}$-mediated signaling in HEK293 cells transiently transfected with $CaSR^{WT}$, $CaSR^{R680G}$, or $CaSR^{L173F}$ (Fig. 4A). The $G_{q/11}$ pathway was first evaluated by measuring the

fold-change accumulation of IP_1, which is a stable metabolite of IP_3 (*23*), in response to alterations in $[Ca^{2+}]_e$. Increasing $[Ca^{2+}]_e$ led to a concentration-dependent fold-change increase in IP_1, which was significantly higher in $CaSR^{L173F}$-expressing cells (68 ± 8), but was not significantly different in $CaSR^{R680G}$-expressing cells (24 ± 5), when compared to $CaSR^{WT}$-expressing cells (30 ± 8) (Fig. 4B). The $G_{q/11}$ pathway was evaluated further by assessing the effects of two inhibitors of the $G_{q/11}$ pathway, YM-254890 and UBO-QIC, both of which selectively block guanosine diphosphate (GDP) dissociation from G_q (*24, 25*), on SRE reporter activity in cells expressing wild-type or mutant CaSRs(Fig. 4C). YM-254890 abolished SRE reporter responses in $CaSR^{WT}$- and $CaSR^{L173F}$-expressing cells (Fig. 4D), but had no effect on $CaSR^{R680G}$-expressing cells (Fig. 4D) when compared to cells expressing $CaSR^{WT}$. Similarly, UBO-QIC significantly decreased SRE reporter responses in $CaSR^{WT}$- and $CaSR^{L173F}$-expressing cells but did not significantly alter responses in $CaSR^{R680G}$-expressing cells (Fig. 4E). These findings indicated that the R680G mutation does not increase signaling through $G_{q/11}$ proteins.

We assessed signaling though the $G_{i/o}$ pathway by measuring cAMP accumulation in cells expressing the wild-type or mutant forms of CaSR (Fig. 5A) in response to increasing $[Ca^{2+}]_e$. A dose-dependent decrease in cAMP was observed in all cells (Fig. 5B), and cells expressing $CaSR^{L173F}$ had a more pronounced cAMP inhibition at 2.5mM $Ca^{2+}{}_e$ and a significantly lower half maximal inhibitory concentration (IC_{50}) value of 1.05mM (95%CI = 0.88-1.22), compared to cells expressing $CaSR^{WT}$ (IC_{50} = 3.11mM (95%CI = 2.88-3.34mM) (Fig. 5C). In contrast, the cAMP responses of cells expressing $CaSR^{R680G}$ (IC_{50} = 3.10mM (95%CI = 2.90-3.30)) did not significantly differ from cells expressing $CaSR^{WT}$ (Fig. 5, B-C). To confirm that the R680G mutation does not enhance MAPK signaling through a $G_{i/o}$-dependent pathway, we also evaluated SRE reporter activity in the presence of pertussis toxin (PTx), which is a selective $G_{i/o}$ inhibitor. Treatment with PTx or vehicle had no effect on the expression of $CaSR^{WT}$, $CaSR^{R680G}$, or $CaSR^{L173F}$ (Fig. 5D). However, addition of PTx led to a similar (>50%) reduction in SRE reporter fold-change responses in both wild-type and mutant CaSR-expressing cells compared to the respective vehicle-treated cells (Fig. 5E), although PTx-treated $CaSR^{R680G}$-expressing cells continued to show significantly increased SRE reporter responses compared to PTx-treated cells expressing $CaSR^{WT}$ (Fig. 5F). Thus, inhibition of $G_{i/o}$-mediated

signaling does not rectify the increased SRE reporter responses caused by the R680G mutation, and overall the combined results indicate that the gain of function associated with the R680G mutation likely involves a mechanism that is independent of $G_{q/11}$ and $G_{i/o}$.

The increased MAPK responses of $CaSR^{R680G}$ are mediated by β-arrestin

To determine whether the increased MAPK signaling responses of cells expressing $CaSR^{R680G}$ may be mediated by a β-arrestin–dependent pathway, we performed SRE reporter assays in the presence of single siRNAs targeting either β-arrestin1 or β-arrestin2 or a scrambled siRNA sequence. Treatment of HEK293 cells transiently expressing $CaSR^{WT}$, $CaSR^{R680G}$, or $CaSR^{L173F}$ with β-arrestin1– or β-arrestin2–targeted siRNA resulted in efficient knockdown of β-arrestin1 and β-arrestin2, respectively, compared to cells treated with scrambled siRNA (fig. S4A-S4B) and did not affect CaSR expression (Fig. 6A and 6B). In the presence of scrambled siRNA, $Ca^{2+}{}_e$-induced SRE reporter fold-change responses in $CaSR^{R680G}$- and $CaSR^{L173F}$-expressing cells were significantly increased compared to cells expressing $CaSR^{WT}$, (Fig. 6, C to F). Treatment with β-arrestin1 or β-arrestin2 siRNA significantly reduced the SRE reporter activity in $CaSR^{WT}$-expressing cells by 20-30% compared to $CaSR^{WT}$-expressing cells treated with scrambled siRNA (Fig. 6C and 6D). Moreover, the knockdown of β-arrestin1 or β-arrestin2 in cells expressing $CaSR^{R680G}$ led to a marked reduction (>80%) in SRE reporter activity compared to the same cells treated with scrambled siRNA (Fig. 6C and 6D). However, the increase in SRE reporter activity of cells expressing $CaSR^{L173F}$ was not altered by knocking down β-arrestin1 or β-arrestin2 (Fig. 6E and 6F). These findings were further evaluated in SRE reporter studies in which cells expressing $CaSR^{WT}$, $CaSR^{R680G}$, or $CaSR^{L173F}$ were exposed to 10mM $[Ca^{2+}]_e$ (fig. S5A and S5B). These experiments showed that β-arrestin1 and β-arrestin2 knockdown reduced SRE responses in cells expressing $CaSR^{R680G}$, such that the SRE fold-change response was either decreased or not significantly different to that of cells expressing $CaSR^{WT}$ (fig. S5A and S5B). Moreover, the addition of NPS-2143 did not further reduce the SRE fold responses in cells expressing $CaSR^{R680G}$ (fig. S5A and S5B). In contrast, knocking down β-arrestin1 or β-arrestin2 in cells expressing $CaSR^{L173F}$ had no effect on SRE fold-change responses when compared to

$CaSR^{WT}$-expressing cells not treated with siRNA, whereas treatment with NPS-2143 rectified these SRE fold-change responses in $CaSR^{L173F}$-expressing cells so that they were similar to those of cells expressing $CaSR^{WT}$ (fig. S5C and S5D). These findings confirm that the Arg^{680} residue is required for NPS-2143 to affect CaSR activity and indicate that signaling through β-arrestins does not represent a general mechanism for ADH1-mediated increases in MAPK responses, but does represent the preferred signaling pathway of $CaSR^{R680G}$.

The R680G mutation disrupts an Arg^{680}-Glu^{767} salt bridge that is required for β-arrestin–mediated CaSR signaling

To determine the mechanism by which the R680G mutation, which is located in the third transmembrane domain (TMD3) of CaSR (Fig. 7A), may influence β-arrestin–mediated signaling, we constructed a homology model of the TMDs and evaluated the structural consequences of the R680G mutation (Fig. 7B–7D). A homology model was chosen because no crystal structure of the TMD of the CaSR exists. We therefore generated a homology model based on the crystal structure of the TMD of the related family C GPCR human metabotropic glutamate receptor 1 (mGluR1) (*26*), which is likely to have a similar structural topology to the CaSR TMD. For the homology modelling we utilized the mGluR1 TMD in complex with the negative allosteric modulator 4-fluoro-*N*-(4-(6-isopropylamino)pyrimidin-4-yl)thiazol-2-yl)-*N*-methylbenzamide (FITM) (*26*). Arg^{680} of CaSR, which is located in the extracellular portion of TMD3, corresponds to Gln^{660} in TMD3 of mGluR1 (Fig. 7C and 7D). The CaSR TMD homology model indicated that the Arg^{680} side chain may potentially form a salt bridge with the side chain of the neighbouring Glu^{767} residue, located in the extracellular loop 2 (ECL2) or, less likely, with the side chain of the more distantly sited Glu^{837} residue, which is located on TMD7 (Fig. 7D). Thus, the R680G mutation likely disrupts a salt bridge between the Arg^{680} and Glu^{767} residues, or possibly a salt bridge between the Arg^{680} and Glu^{837} residues. CaSR mutations of both the Glu^{767} and Glu^{837} residues have previously been shown to increase signaling by the CaSR (*26-29*), and we therefore postulated that the β-arrestin–mediated

increase in MAPK signaling caused by the R680G mutation may result from the disruption of a salt bridge between Arg^{680} and either Glu^{767} or Glu^{837}.

To test this hypothesis we mutated the Glu^{767} and Glu^{837} residues to Arg (E767R and E837R, respectively), because this would allow us to determine whether reversing the residue charge, which would cause a switch from a favorable salt bridge to unfavourable electrostatic interaction with Arg^{680}, would affect β-arrestin–mediated CaSR signaling. The effect of the E767R and E837R mutations on MAPK signaling downstream of CaSR was initially assessed by Western blot analysis of ERK1/2 phosphorylation in response to treatment of cells with 0mM and 5mM Ca^{2+}_e. The abundance of phosphorylated ERK1/2 in response to 5mM Ca^{2+}_e was similar in cells expressing $CaSR^{WT}$ and $CaSR^{E837R}$ (fig. S6A-S6D and fig. S7A-S7D). However, cells expressing $CaSR^{E767R}$ had significantly more ERK1/2 phosphorylation compared to cells expressing $CaSR^{WT}$, consistent with a gain of function (fig. S6 and fig. S7). These findings were further evaluated in SRE reporter studies in cells treated with siRNAs targeting β-arrestins. Expression of the CaSRs was confirmed by Western blot analysis (Fig. 8A and 8B). In the presence of scrambled siRNA, Ca^{2+}_e-induced SRE reporter activity in cells expressing $CaSR^{E767R}$ was significantly increased compared to cells expressing $CaSR^{WT}$, whereas cells expressing $CaSR^{E837R}$ had SRE reporter responses similar to cells expressing $CaSR^{WT}$ (Fig. 8C and 8D). Moreover, treatment with siRNAs targeting β-arrestin1 or β-arrestin2 had no effect on SRE responses in cells expressing $CaSR^{E837R}$ (Fig. 8C and 8D) or $CaSR^{WT}$, except when the cells were treated with 10mM Ca^{2+}_e. These results indicate that Glu^{837} is unlikely to be involved in forming a salt bridge with Arg^{680} or other adjacent residues (fig. S8A-S8B), and that mutations of Glu^{837} are likely to alter CaSR function by another mechanism.

In contrast, SRE reporter activity decreased significantly upon knockdown of β-arrestin1 or β-arrestin2 in cells expressing $CaSR^{E767R}$ in the presence of 2.5-10mM Ca^{2+}_e, compared to the same cells treated with scrambled siRNA (Fig. 8C and 8D). These findings indicate that, similar to the R680G mutation, the E767R mutation significantly increased CaSR-induced MAPK signaling through a β-arrestin–mediated pathway and that Glu^{767} was likely required to form a salt bridge with Arg^{680}. To confirm that the Arg^{680}-Glu^{767} salt bridge was required for MAPK signaling, we generated a double-

mutant CaSR, in which the Arg^{680} residue was mutated to Glu^{680} (R680E) and the Glu^{767} (E767R) residue was mutated to Arg^{767} (E767R). This Glu^{680}-Arg^{767} double-mutant CaSR ($CaSR^{R680E-E767R}$) was predicted to form a salt bridge between residues 680 and 767, and thus mediate MAPK signaling similar to $CaSR^{WT}$. To determine the effect of the combined mutations on MAPK signaling, we initially assessed ERK1/2 phosphorylation by Western blot analysis (fig. S6 and fig. S9A-S9D), after confirming expression of CaSR by Western blot analysis of lysates from cells expressing wild-type and mutant CaSRs (Fig. 8E and 8F). The abundance of phosphorylated ERK1/2 in response to 5mM Ca^{2+}_e was similar in cells expressing $CaSR^{WT}$ and cells expressing the double mutant Glu^{680}-Arg^{767} form of CaSR (fig. S6 and fig. S9). SRE reporter responses did not differ significantly between cells expressing the wild-type and double mutant forms of CaSR, and knockdown of β-arrestin1 or β-arrestin2 only reduced SRE reporter responses in the presence of 10mM Ca^{2+}_e, similarly to cells expressing $CaSR^{WT}$ (Fig. 8G and 8H). Thus, these double mutant studies demonstrated the importance of the salt bridge between residues 680 and 767 for CaSR-induced MAPK signaling.

DISCUSSION

Our studies have identified a previously undescribed ADH1-causing mutation affecting the CaSR (R680G), which causes a biased signaling response to Ca^{2+}_e and leads to a gain-of-function in MAPK signaling without altering Ca^{2+}_i responses (Figs. 2, 3 and 6). The effect of this mutation contrasts with the majority of mutations associated with ADH1, which bias the CaSR towards Ca^{2+}_i signaling (*11*). The CaSR is most abundant in the parathyroid glands (*30*), and the demonstration that the R680G CaSR mutation leads to selective MAPK activation suggests that this signaling pathway may influence the parathyroid set-point for PTH release. Thus, the hypocalcemia in the family harboring this CaSR mutation may have been caused by the MAPK pathway increasing the sensitivity of parathyroid cells to Ca^{2+}_e, which impaired the synthesis and release of PTH at physiological Ca^{2+}_e concentrations. Consistent with this, an *ex-vivo* study has previously shown alterations in MAPK activity to acutely influence PTH secretion from cultured human parathyroid cells (*31*). However, the physiological significance of CaSR-mediated biased signaling leading to MAPK activation remains to

be elucidated. Furthermore, our studies have revealed the importance of functionally characterizing CaSR variants by measuring both Ca^{2+}_i and MAPK signaling responses because the R680G mutation may have been mistakenly classified as a benign polymorphism if only the Ca^{2+}_i activity downstream of this mutant receptor had been assessed. Therefore, CaSR variants previously detected in hypocalcemic and hypercalcemic probands and classified as polymorphisms may require further evaluation to ensure that biased signaling is not a feature of these variants.

Our studies also reveal that the Arg^{680} residue is critical for the binding and efficacy of the allosteric CaSR modulator NPS-2143. Allosteric CaSR modulators have been predicted to bind to a cavity formed by the extracellular portions of the CaSR TMDs (*18*), and it is noteworthy that the Arg^{680} residue is located at the entrance to this putative binding cavity. Moreover, the NPS-2143 calcilytic compound is predicted to bind to this cavity, and our results showing that the CaSR R680G mutation abolishes NPS-2143–mediated Ca^{2+}_i and MAPK responses demonstrate the importance of the CaSR Arg^{680} residue in mediating the action of this calcilytic drug (*18*).

The CaSR has previously been shown to activate the MAPK cascade through $G_{q/11}$ and $G_{i/o}$ (*5*), and in keeping with this, our analysis of the reported ADH1-causing L173F CaSR mutant showed this to enhance MAPK signaling through $G_{q/11}$ and $G_{i/o}$ (Fig. 3 to 5). Thus, two inhibitors of the $G_{q/11}$ pathway, YM-254890 and UBO-QIC, and PTx, a selective inhibitor of $G_{i/o}$, abolished and reduced, respectively, the enhanced MAPK signaling associated with the L173F mutant CaSR (Fig. 4 and 5). In contrast, assessment of the newly identified ADH1-causing R680G mutant CaSR using the $G_{q/11}$ and $G_{i/o}$ inhibitors revealed that the associated increased MAPK signaling remained significantly increased compared to the MAPK signaling in similarly treated cells expressing wild-type CaSR (Fig. 4 and 5), although it was reduced when compared to untreated cells expressing the G680 CaSR mutant (Fig. 4 and 5). However, the increased MAPK signaling due to the R680 mutation, but not that due to the F173 mutation, was significantly reduced by knockdown of β-arrestin1 or β-arrestin2 when compared to similarly treated cells expressing wild-type CaSR (Fig. 4 and 5). Taken together, these results indicate that the gain-of-function F173 mutant CaSR signals through the canonical $G_{q/11}$ and $G_{i/o}$ pathways, but the gain-of-function G680 mutant CaSR signals through the canonical pathways as

well as a non-canonical pathway that is independent of $G_{q/11}$ and $G_{i/o}$ and involves the β-arrestin proteins (Fig. 6).

The β-arrestins may enhance ERK1/2 signaling by acting as protein scaffolds that mediate the association of ERK1/2 with upstream MAPK components such as Raf-1 and the MAPK and ERK kinases 1 and 2 (MEK1/2) (*32*). The assembly of the β-arrestin–MAPK complex is triggered by GPCR activation and occurs after agonist-bound GPCRs have undergone clathrin-mediated endocytosis (*33*). Thus, CaSR endocytosis is likely required to mediate β-arrestin–dependent MAPK activation, and this is consistent with our reported finding of impaired CaSR-MAPK signaling due to FHH3-associated loss-of-function mutations of the adaptor-related protein 2 σ-subunit (AP2σ), which mediates the formation of clathrin-coated vesicles (*21*). Moreover, our present study has revealed that β-arrestins 1 and 2 mediated the gain of function caused by the R680G CaSR mutation (Fig. 6), and it is of note that both of these β-arrestin isoforms, which are present in parathyroid glands, have been reported by co-immunoprecipitation and mammalian two-hybrid assays to directly bind to the CaSR cytoplasmic terminus (*34*).

The role of β-arrestins in GPCR endocytosis and signal transduction has been characterized (*7, 32*), although the GPCR domains and structural motifs that mediate these interactions with β-arrestins have not been fully elucidated. A crystal structure analysis of the GPCR family A member β2-adrenergic receptor (β2-AR) complexed with β-arrestin 1 has shown that the GPCR cytoplasmic terminus, third intracellular loop, and inner membrane aspect of the TMDs facilitate β-arrestin binding to the GPCR (*35*). In addition, mutations affecting the cytoplasmic regions of family A and B GPCRs have been shown to selectively influence β-arrestin–mediated signaling (*36, 37*). Our finding that mutation of the CaSR Arg^{680} residue, which is located at the outer end of TMD3 (Fig. 7), also modulates β-arrestin signaling, reveals the importance of the extracellular regions of GPCRs for influencing β-arrestin function. Our homology modeling and functional analysis of engineered CaSR mutants has revealed that the Arg^{680} residue forms a salt bridge with the Glu^{767} residue located in ECL2 (Fig. 8) and that this salt bridge likely maintains the CaSR in an inactive conformation. Indeed, disruption of this salt bridge by mutating either Arg^{680} or Glu^{767} led to a gain of function in β-arrestin–

mediated MAPK signaling, whereas restoration of the salt bridge in the Glu^{680}-Arg^{767} double mutant normalized CaSR function (Fig. 8). The Arg^{680}-Glu^{767} salt bridge therefore mediates a functionally important interaction between TMD3 and ECL2 (Fig. 7 and 8). ECL2 connects the outer ends of TMD4 and TMD5 (Fig. 7A and 7B), and thus it seems likely that disruption of the Arg^{680}-Glu^{767} salt bridge may lead to a lateral displacement of TMD3 away from TMD4 or TMD5, thereby facilitating β-arrestin binding in a manner analogous to that reported in a cryo-EM structural analysis of the β2-AR–β-arrestin complex, which showed that binding of β-arrestin to the β2-AR TMD domain core region is mediated by an outward shift in the positioning of the TMD3, TMD5, and TMD6 helices (*35*).

In conclusion, we have identified a CaSR mutation (R680G) that gives rise to ADH1 by exclusively activating a β-arrestin–mediated MAPK signaling pathway downstream of the CaSR. These studies provide key insights into CaSR structure and function and indicate that a salt bridge between TMD3 and ECL2 plays a critical role in the control of β-arrestin–mediated CaSR signaling. Moreover, discovery of this novel β-arrestin–specific pathway may help facilitate the development of targeted therapeutics that can activate CaSR-mediated β-arrestin signaling in a biased manner.

MATERIALS AND METHODS

DNA sequence analysis

Written informed consent was obtained from the individuals and their relatives, and where appropriate the parents and guardians of children, using protocols approved by local and national ethics committees. Mutational analysis of the *CASR* exons and adjacent splice-sites was performed as described (*38*). Publicly accessible databases (dbSNP (http://www.ncbi.nlm.nih.gov/projects/SNP/) (*39*); 1000 genomes (http://browser.1000genomes.org) (*40*); the National Heart, Lung and Blood Institute (NHLBI) Exome Sequencing Project (http://evs.gs.washington.edu/EVS/, EVS data release ESP6500SI) with details from the exomes of approximately 6500 individuals; and the Exome Aggregation Consortium (ExAC) (exac.broadinstitute.org) with details from exomes of 60,706 unrelated individuals (*41*)), were examined for the presence of the c.2038C>G sequence variant.

Protein sequence analysis and alignment and three-dimensional modeling of the CaSR structure

The effect of the R680G mutation was predicted using Polyphen-2 (http://genetics.bwh.harvard.edu/pph2/) (*13*) and MutationTasting (http://www.mutationtaster.org/) (*14*). Protein sequences of CaSR orthologs were aligned using ClustalOmega (http://www.ebi.ac.uk/Tools/msa/clustalo/) (*42*). The HHpred homology detection server (https://toolkit.tuebingen.mpg.de/hhpred) was used to identify proteins in the Protein Data Bank with structural similarity to the CaSR and to perform amino acid sequence alignment (*43*). The amino acid sequence identity between human metabotropic glutamate receptor 1 (mGluR1)(*44*) and the CaSR is 28% for 282 aligned amino acid residues. The CaSR sequence was threaded onto the mGluR1 template coordinates, and Modeller (https://toolkit.tuebingen.mpg.de/modeller) was used to construct a homology model (*45*). Figures were prepared using the PyMOL Molecular Graphics System (Schrodinger, LLC).

Cell culture, transfection, and siRNA-mediated knockdown

Studies were performed in HEK293 cells maintained in DMEM-Glutamax media (ThermoFisher) with 10% fetal bovine serum (Gibco) at 37ºC, 5% CO_2. Mutations were introduced into the pEGFP-N1-CaSR^{WT} construct by site-directed mutagenesis using the Quikchange Lightning Kit (Agilent Technologies) and gene-specific primers (SigmaAldrich) as described (*46, 47*), Engineered mutations were verified using dideoxynucleotide sequencing with the BigDye Terminator v3.1 cycle sequencing kit (Life Technologies) and an automated detection system (ABI3730 automated capillary sequencer; Applied Biosystems) as previously reported (*48*). Wild-type and mutant CaSR pEGFP-N1 constructs, and luciferase reporter constructs (pGL4.30-NFAT and pGL4.33-SRE, Promega) were transiently transfected into HEK293 cells using Lipofectamine 2000 (LifeTechnologies) 48 hours before experiments, as described (*49*). Single siRNAs targeted to β-arrestin1 (Catalog No: 6218S, Cell Signalling Technology) or β-arrestin2 (Catalog No: sc29208, SantaCruz Biotechnology), or scrambled siRNA (Catalog No: SR301839, Origene) were transfected 24 hours before experiments at a concentration of 100nM. Successful transfection was confirmed by Western blot analysis, with the calnexin housekeeping protein being used as a loading control (*46*). Primary antibodies recognizing the following proteins were used for Western blot analysis at a dilution of 1:1000: CaSR (ADD, ab19347, Abcam), calnexin (Ab2301, Millipore), phosphorylated ERK1/2 (9101L, Cell Signaling Technology), total ERK1/2 (4695S, clone 137F5, Cell Signaling Technology), plasma membrane calcium ATPase (PMCA1) (ab190355, Abcam), β-arrestin1 (ab175266, Abcam), and β-arrestin2 (H-9, sc-13140, SantaCruz). The Western blots were visualized using an Immuno-Star WesternC kit (BioRad) on a BioRad Chemidoc XRS+ system (*46*). For cell fractionation studies, cells were transfected with CaSR constructs and 48 hours later plasma membrane and cytoplasmic fractions were isolated using a plasma membrane extraction kit (Catalog No 65400, Abcam), as described (*50*). Plasma membrane fractions were dissolved in 0.5% Triton-X100 in PBS, and the cytoplasmic fraction in the supplied homogenization buffer. Each fraction was resuspended in Laemmli buffer and Western blot analysis performed, as described (*48*). Calnexin was used as a loading control for cytoplasmic fractions, and the PMCA1 protein used as a loading control for plasma membrane fractions. For studies of phosphorylated proteins, cells were treated for 5 minutes with either 0mM or 5mM Ca^{2+}_e,

prior to lysis and proteins separated by SDS-PAGE. Following transfer to polyvinylidene difluoride (PVDF) membranes, blots were pre-incubated (blocked) in 5% bovine serum albumin (BSA) in Tris-buffered saline with Tween-20 (TBSt) (Sigma) prior to probing for phosphorylated ERK. Blots were stripped with Restore Plus Western Blot Stripping Buffer (ThermoFisher) for 15 min, and then blocked in non-fat dried milk powder (commercially available as Marvel) dissolved in TBSt and reprobed for total ERK. Densitometry was performed using ImageJ 1.30 software (NIH, USA) and analysed using GraphPad Prism software (GraphPad software) and are expressed as mean±SEM. For studies involving NPS-2143 (ab145050, Abcam), cells were either incubated with DMSO (vehicle) or with 500 nM NPS-2143 in DMSO at 30 min prior to undertaking Fluo-4 $Ca^{2+}{}_i$ experiments (*18*), and for four hours prior to undertaking luciferase reporter assay experiments (*49*).

Surface biotinylation experiments

Biotinylation assays were performed by adapting previously published methods (*51*). Briefly, HEK293 cells were grown in T75 flasks and transiently transfected with 8 µg wild-type or mutant CaSR constructs. Forty-eight hours later cells were biotinylated using the membrane-impermeant sulfo-NHS-SS-biotin (Pierce, 2.5 mg/ml in PBS) for 30 minutes on ice. Cells were then rinsed with ice-cold PBS plus 100mM glycine, and solubilized in cell lysis buffer (150mM NaCl, 50mM Tris-HCl, pH 7.4, 1mM EDTA, 1% Triton X-100) supplemented with 1 tablet of cOmplete, EDTA-free protease inhibitor cocktail (Roche). Cells were lysed for 1 hour at 4°C, pelleted at 13,000 x *g* for 15 minutes, and biotinylated proteins isolated by incubation with streptavidin-agarose beads (Pierce) overnight at 4°C on a rotating wheel. Precipitates were washed with lysis buffer, and biotinylated proteins were eluted from beads using Laemmli buffer. Biotinylated proteins were then resolved by SDS-PAGE and probed for CaSR as described above. A 1:10 dilution of total protein was resolved alongside biotinylated proteins as a control. Specificity of surface biotinylation was confirmed by the absence of the intracellular calnexin in the biotinylated fraction, but presence in total protein fractions. Densitometry was performed using ImageJ 1.30 software (NIH, USA) and analysed using GraphPad Prism software (GraphPad software) and are expressed as mean±SEM.

Intracellular calcium measurements

Ca^{2+}_e-induced Ca^{2+}_i responses were measured by Fluo-4 calcium assays adapted from previously reported methods (*18*). Briefly, CaSR-expressing HEK cells were plated in poly-L-lysine–treated black-walled 96-well plates (Corning), and transiently transfected with 1000ng/ml pBI-CMV2-*GNA11*. On the following day, cells were incubated in serum-free media for 2 hours, then loaded with Fluo-4 dye according to manufacturer's instructions (Invitrogen). Cells were loaded for 40 minutes at 37°C, then either a 20% aqueous solution of 2-hydoxypropyl-β-cyclodextrin (vehicle) or 500 nM NPS-2143 was added. Cells were then incubated for a further 20 minutes at 37°C (*18*). Baseline measurements were made and increasing doses of $CaCl_2$ (0-10 mM) injected into each well using an automated system. Changes in Ca^{2+}_i were recorded on a PHERAstar instrument (BMG Labtech) at 37°C with an excitation filter of 485nm and an emission filter of 520nm. The peak mean fluorescence ratio of the transient response after each individual stimulus was measured using MARS data analysis software (BMG Labtech) and expressed as a normalized response. Nonlinear regression of concentration-response curves was performed with GraphPad Prism using the normalized response at each $[Ca^{2+}]_e$ for each separate experiment and used to determine the EC_{50} (i.e. $[Ca^{2+}]_e$ required for 50% of the maximal response). Assays were performed in 4 biological replicates for each of the expression constructs. Statistical analysis was performed using the *F*-test (*52, 53*).

Luciferase reporter assays

Luciferase reporter assays were undertaken to measure SRE and NFAT responses. Cells were plated in 24-well plates and transiently transfected with 100ng/ml of the wild-type or mutant CaSR pEGFP-N1 constructs, 100ng/ml luciferase construct (either pGL4-NFAT or pGL4-SRE), and 10ng/ml pRL. At 48 hours after transfection, cells were incubated in serum-free media overnight. Cells were then incubated in serum-free media containing 0-10mM $CaCl_2$ for 4 hours. For studies with pertussis toxin (PTx, Catalog No: P7208, Sigma), cells were pre-incubated with 10μM forskolin (MP Biomedicals) overnight, then 300ng/ml PTx, or ethanol-diluent vehicle (Sigma) added with 0-10 mM $CaCl_2$ (*54*).

For studies with $G_{q/11}$ inhibitors, cells were pre-treated with 10μM YM-254890 or vehicle (DMSO) for 5 minutes, or with 1μM UBO-QIC or vehicle (DMSO) for 2 hours. Cells were lysed and assays performed using Dual-Glo Luciferase (Promega) on a Veritas Luminometer (Promega), as previously described (*48*). Luciferase:renilla ratios are shown as fold-changes relative to responses at basal $CaCl_2$ concentrations (0.1mM). Area under the curve (AUC) was calculated using GraphPad Prism and expressed as mean±SEM.

AlphaScreen assays

AlphaScreen assays to measure phosphorylated ERK 1/2 and cAMP were performed in 48-well plates using cells transiently transfected with 100ng of the wild-type or mutant CaSR pEGFP-N1 constructs 48-hours prior to performance of assays. For phosphorylated ERK 1/2 studies, cells were incubated in serum-free media for 12 hours prior to 5-minute treatment with 0.1-10mM $CaCl_2$. Cells were then lysed in Surefire lysis buffer (Perkin Elmer), and phosphorylated ERK 1/2 and total ERK1/2 assays were performed as previously described (*21*). For the cAMP assays, cells were treated with 10μM forskolin for 30 minutes prior to $CaCl_2$ treatment in stimulation buffer [1x Hanks Buffered Saline Solution, 0.1% BSA, 0.1% 3-isobutyl-1-methylxanthine (IBMX), 0.5mM HEPES] plus 0.1-10mM $CaCl_2$. Cells were incubated for 15 minutes, then lysed in a HEPES-based solution (0.1% BSA, 0.3% Tween-20, 5mM HEPES, pH7.4) and incubated for 4 hours. The fluorescence signal in AlphaScreen assays was measured using the PHERAstar FS microplate reader (BMG Labtech) (*48*). Nonlinear regression of concentration-response curves was performed with GraphPad Prism for the determination of IC_{50} (i.e., $[Ca^{2+}]_e$ required for 50% inhibition of the maximal response).

IP_1 assay

Assays were performed in 48-well plates and cells transiently transfected with 100ng of the wild-type or mutant CaSR pEGFP-N1 constructs 48 hours prior to performance of assays. At 24 hours prior to experiments, cells were re-plated in a 384-well plate, and 12-hours later, the media was changed to serum-free media. IP-One homogenous time-resolved fluorescence (HTRF) assays (Cisbio, Codolet, France) were performed according to manufacturer's instructions and as previously described (*23*).

Cells were incubated for 30 minutes with stimulation buffer containing a single dose of $CaCl_2$ (0.1-10mM), followed by lysis in the manufacturer-supplied lysis buffer. Plates were read on a PHERAStar FS microplate reader one hour later (BMG Labtech).

Statistical analysis

A minimum of four independent biological replicates were used for all statistical comparisons. EC_{50} and IC_{50} values were analysed using the *F*-test, as reported (*53*). All other data was analyzed by 2-way ANOVA with Tukey's multiple-comparisons test. Statistical analyses were undertaken using GraphPad Prism (GraphPad), and a value of $p<0.05$ was considered significant for all analyses.

SUPPLEMENTARY MATERIALS

REFERENCES AND NOTES

1. E. M. Brown, Role of the calcium-sensing receptor in extracellular calcium homeostasis. *Best practice & research. Clinical endocrinology & metabolism* **27**, 333-343 (2013).
2. W. Chang, T. H. Chen, S. Pratt, D. Shoback, Amino acids in the second and third intracellular loops of the parathyroid Ca2+-sensing receptor mediate efficient coupling to phospholipase C. *The Journal of biological chemistry* **275**, 19955-19963 (2000).
3. M. A. Goolam, J. H. Ward, V. A. Avlani, K. Leach, A. Christopoulos, A. D. Conigrave, Roles of intraloops-2 and -3 and the proximal C-terminus in signalling pathway selection from the human calcium-sensing receptor. *FEBS letters* **588**, 3340-3346 (2014).
4. A. M. Hofer, E. M. Brown, Extracellular calcium sensing and signalling. *Nature reviews. Molecular cell biology* **4**, 530-538 (2003).
5. O. Kifor, R. J. MacLeod, R. Diaz, M. Bai, T. Yamaguchi, T. Yao, I. Kifor, E. M. Brown, Regulation of MAP kinase by calcium-sensing receptor in bovine parathyroid and CaR-transfected HEK293 cells. *Am J Physiol Renal Physiol* **280**, F291-302 (2001).
6. A. R. Thomsen, M. Hvidtfeldt, H. Brauner-Osborne, Biased agonism of the calcium-sensing receptor. *Cell calcium* **51**, 107-116 (2012).
7. A. K. Shukla, K. Xiao, R. J. Lefkowitz, Emerging paradigms of beta-arrestin-dependent seven transmembrane receptor signaling. *Trends in biochemical sciences* **36**, 457-469 (2011).
8. K. Eichel, D. Jullie, M. von Zastrow, beta-Arrestin drives MAP kinase signalling from clathrin-coated structures after GPCR dissociation. *Nature cell biology* **18**, 303-310 (2016).
9. S. H. Pearce, C. Williamson, O. Kifor, M. Bai, M. G. Coulthard, M. Davies, N. Lewis-Barned, D. McCredie, H. Powell, P. Kendall-Taylor, E. M. Brown, R. V. Thakker, A familial syndrome of hypocalcemia with hypercalciuria due to mutations in the calcium-sensing receptor. *N Engl J Med* **335**, 1115-1122 (1996).
10. F. Raue, J. Pichl, H. G. Dorr, D. Schnabel, P. Heidemann, G. Hammersen, C. Jaursch-Hancke, R. Santen, C. Schofl, M. Wabitsch, C. Haag, E. Schulze, K. Frank-Raue, Activating mutations in the calcium-sensing receptor: genetic and clinical spectrum in 25 patients with autosomal dominant hypocalcaemia - a German survey. *Clinical endocrinology* **75**, 760-765 (2011).
11. K. Leach, A. Wen, A. E. Davey, P. M. Sexton, A. D. Conigrave, A. Christopoulos, Identification of molecular phenotypes and biased signaling induced by naturally occurring mutations of the human calcium-sensing receptor. *Endocrinology* **153**, 4304-4316 (2012).
12. K. Leach, A. Wen, A. E. Cook, P. M. Sexton, A. D. Conigrave, A. Christopoulos, Impact of clinically relevant mutations on the pharmacoregulation and signaling bias of the calcium-sensing receptor by positive and negative allosteric modulators. *Endocrinology* **154**, 1105-1116 (2013).
13. I. Adzhubei, D. M. Jordan, S. R. Sunyaev, Predicting functional effect of human missense mutations using PolyPhen-2. *Current protocols in human genetics* **Chapter 7**, Unit7 20 (2013).
14. J. M. Schwarz, D. N. Cooper, M. Schuelke, D. Seelow, MutationTaster2: mutation prediction for the deep-sequencing age. *Nature methods* **11**, 361-362 (2014).
15. S. U. Miedlich, L. Gama, K. Seuwen, R. M. Wolf, G. E. Breitwieser, Homology modeling of the transmembrane domain of the human calcium sensing receptor and localization of an allosteric binding site. *The Journal of biological chemistry* **279**, 7254-7263 (2004).
16. F. M. Hannan, M. A. Nesbit, C. Zhang, T. Cranston, A. J. Curley, B. Harding, C. Fratter, N. Rust, P. T. Christie, J. J. Turner, M. C. Lemos, M. R. Bowl, R. Bouillon, C. Brain, N. Bridges, C. Burren, J. M. Connell, H. Jung, E. Marks, D. McCredie, Z. Mughal, C. Rodda, S. Tollefsen, E. M. Brown, J. J. Yang, R. V. Thakker, Identification of 70 calcium-sensing receptor mutations in hyper- and hypo-calcaemic patients: evidence for clustering of extracellular domain mutations at calcium-binding sites. *Human molecular genetics* **21**, 2768-2778 (2012).
17. E. White, J. McKenna, A. Cavanaugh, G. E. Breitwieser, Pharmacochaperone-mediated rescue of calcium-sensing receptor loss-of-function mutants. *Molecular endocrinology* **23**, 1115-1123 (2009).
18. K. Leach, K. J. Gregory, I. Kufareva, E. Khajehali, A. E. Cook, R. Abagyan, A. D. Conigrave, P. M. Sexton, A. Christopoulos, Towards a structural understanding of allosteric drugs at the human calcium-sensing receptor. *Cell research* **26**, 574-592 (2016).

19. F. M. Hannan, G. V. Walls, V. N. Babinsky, M. A. Nesbit, E. Kallay, T. A. Hough, W. D. Fraser, R. D. Cox, J. Hu, A. M. Spiegel, R. V. Thakker, The Calcilytic Agent NPS 2143 Rectifies Hypocalcemia in a Mouse Model With an Activating Calcium-Sensing Receptor (CaSR) Mutation: Relevance to Autosomal Dominant Hypocalcemia Type 1 (ADH1). *Endocrinology* **156**, 3114-3121 (2015).
20. L. A. Timmerman, N. A. Clipstone, S. N. Ho, J. P. Northrop, G. R. Crabtree, Rapid shuttling of NF-AT in discrimination of Ca2+ signals and immunosuppression. *Nature* **383**, 837-840 (1996).
21. V. N. Babinsky, F. M. Hannan, C. M. Gorvin, S. A. Howles, M. A. Nesbit, N. Rust, A. C. Hanyaloglu, J. Hu, A. M. Spiegel, R. V. Thakker, Allosteric Modulation of the Calcium-sensing Receptor Rectifies Signaling Abnormalities Associated with G-protein alpha-11 Mutations Causing Hypercalcemic and Hypocalcemic Disorders. *The Journal of biological chemistry* **291**, 10876-10885 (2016).
22. D. Li, E. E. Opas, F. Tuluc, D. L. Metzger, C. Hou, H. Hakonarson, M. A. Levine, Autosomal dominant hypoparathyroidism caused by germline mutation in GNA11: phenotypic and molecular characterization. *J Clin Endocrinol Metab* **99**, E1774-1783 (2014).
23. C. Zhang, N. Mulpuri, F. M. Hannan, M. A. Nesbit, R. V. Thakker, D. Hamelberg, E. M. Brown, J. J. Yang, Role of Ca2+ and L-Phe in regulating functional cooperativity of disease-associated "toggle" calcium-sensing receptor mutations. *PloS one* **9**, e113622 (2014).
24. A. Nishimura, K. Kitano, J. Takasaki, M. Taniguchi, N. Mizuno, K. Tago, T. Hakoshima, H. Itoh, Structural basis for the specific inhibition of heterotrimeric Gq protein by a small molecule. *Proceedings of the National Academy of Sciences of the United States of America* **107**, 13666-13671 (2010).
25. J. P. Kukkonen, G-protein inhibition profile of the reported Gq/11 inhibitor UBO-QIC. *Biochemical and biophysical research communications* **469**, 101-107 (2016).
26. J. Hu, S. J. McLarnon, S. Mora, J. Jiang, C. Thomas, K. A. Jacobson, A. M. Spiegel, A region in the seven-transmembrane domain of the human Ca2+ receptor critical for response to Ca2+. *The Journal of biological chemistry* **280**, 5113-5120 (2005).
27. J. Hu, G. Reyes-Cruz, W. Chen, K. A. Jacobson, A. M. Spiegel, Identification of acidic residues in the extracellular loops of the seven-transmembrane domain of the human Ca2+ receptor critical for response to Ca2+ and a positive allosteric modulator. *The Journal of biological chemistry* **277**, 46622-46631 (2002).
28. A. Uckun-Kitapci, L. E. Underwood, J. Zhang, B. Moats-Staats, A novel mutation (E767K) in the second extracellular loop of the calcium sensing receptor in a family with autosomal dominant hypocalcemia. *American journal of medical genetics. Part A* **132A**, 125-129 (2005).
29. J. Hu, J. Jiang, S. Costanzi, C. Thomas, W. Yang, J. H. Feyen, K. A. Jacobson, A. M. Spiegel, A missense mutation in the seven-transmembrane domain of the human Ca2+ receptor converts a negative allosteric modulator into a positive allosteric modulator. *The Journal of biological chemistry* **281**, 21558-21565 (2006).
30. J. B. Regard, I. T. Sato, S. R. Coughlin, Anatomical profiling of G protein-coupled receptor expression. *Cell* **135**, 561-571 (2008).
31. S. Corbetta, A. Lania, M. Filopanti, L. Vicentini, E. Ballare, A. Spada, Mitogen-activated protein kinase cascade in human normal and tumoral parathyroid cells. *J Clin Endocrinol Metab* **87**, 2201-2205 (2002).
32. S. M. DeWire, S. Ahn, R. J. Lefkowitz, S. K. Shenoy, Beta-arrestins and cell signaling. *Annual review of physiology* **69**, 483-510 (2007).
33. Y. Daaka, L. M. Luttrell, S. Ahn, G. J. Della Rocca, S. S. Ferguson, M. G. Caron, R. J. Lefkowitz, Essential role for G protein-coupled receptor endocytosis in the activation of mitogen-activated protein kinase. *The Journal of biological chemistry* **273**, 685-688 (1998).
34. M. Pi, R. H. Oakley, D. Gesty-Palmer, R. D. Cruickshank, R. F. Spurney, L. M. Luttrell, L. D. Quarles, Beta-arrestin- and G protein receptor kinase-mediated calcium-sensing receptor desensitization. *Molecular endocrinology* **19**, 1078-1087 (2005).
35. A. K. Shukla, G. H. Westfield, K. Xiao, R. I. Reis, L. Y. Huang, P. Tripathi-Shukla, J. Qian, S. Li, A. Blanc, A. N. Oleskie, A. M. Dosey, M. Su, C. R. Liang, L. L. Gu, J. M. Shan, X. Chen, R. Hanna, M. Choi, X. J. Yao, B. U. Klink, A. W. Kahsai, S. S. Sidhu, S. Koide, P. A. Penczek,

A. A. Kossiakoff, V. L. Woods, Jr., B. K. Kobilka, G. Skiniotis, R. J. Lefkowitz, Visualization of arrestin recruitment by a G-protein-coupled receptor. *Nature* **512**, 218-222 (2014).
36. Y. Yin, X. E. Zhou, L. Hou, L. H. Zhao, B. Liu, G. Wang, Y. Jiang, K. Melcher, H. E. Xu, An intrinsic agonist mechanism for activation of glucagon-like peptide-1 receptor by its extracellular domain. *Cell discovery* **2**, 16042 (2016).
37. K. M. Kim, M. G. Caron, Complementary roles of the DRY motif and C-terminus tail of GPCRS for G protein coupling and beta-arrestin interaction. *Biochemical and biophysical research communications* **366**, 42-47 (2008).
38. P. H. Nissen, S. E. Christensen, L. Heickendorff, K. Brixen, L. Mosekilde, Molecular genetic analysis of the calcium sensing receptor gene in patients clinically suspected to have familial hypocalciuric hypercalcemia: phenotypic variation and mutation spectrum in a Danish population. *J Clin Endocrinol Metab* **92**, 4373-4379 (2007).
39. S. T. Sherry, M. H. Ward, M. Kholodov, J. Baker, L. Phan, E. M. Smigielski, K. Sirotkin, dbSNP: the NCBI database of genetic variation. *Nucleic acids research* **29**, 308-311 (2001).
40. C. Genomes Project, A. Auton, L. D. Brooks, R. M. Durbin, E. P. Garrison, H. M. Kang, J. O. Korbel, J. L. Marchini, S. McCarthy, G. A. McVean, G. R. Abecasis, A global reference for human genetic variation. *Nature* **526**, 68-74 (2015).
41. M. Lek, K. J. Karczewski, E. V. Minikel, K. E. Samocha, E. Banks, T. Fennell, A. H. O'Donnell-Luria, J. S. Ware, A. J. Hill, B. B. Cummings, T. Tukiainen, D. P. Birnbaum, J. A. Kosmicki, L. E. Duncan, K. Estrada, F. Zhao, J. Zou, E. Pierce-Hoffman, J. Berghout, D. N. Cooper, N. Deflaux, M. DePristo, R. Do, J. Flannick, M. Fromer, L. Gauthier, J. Goldstein, N. Gupta, D. Howrigan, A. Kiezun, M. I. Kurki, A. L. Moonshine, P. Natarajan, L. Orozco, G. M. Peloso, R. Poplin, M. A. Rivas, V. Ruano-Rubio, S. A. Rose, D. M. Ruderfer, K. Shakir, P. D. Stenson, C. Stevens, B. P. Thomas, G. Tiao, M. T. Tusie-Luna, B. Weisburd, H. H. Won, D. Yu, D. M. Altshuler, D. Ardissino, M. Boehnke, J. Danesh, S. Donnelly, R. Elosua, J. C. Florez, S. B. Gabriel, G. Getz, S. J. Glatt, C. M. Hultman, S. Kathiresan, M. Laakso, S. McCarroll, M. I. McCarthy, D. McGovern, R. McPherson, B. M. Neale, A. Palotie, S. M. Purcell, D. Saleheen, J. M. Scharf, P. Sklar, P. F. Sullivan, J. Tuomilehto, M. T. Tsuang, H. C. Watkins, J. G. Wilson, M. J. Daly, D. G. MacArthur, C. Exome Aggregation, Analysis of protein-coding genetic variation in 60,706 humans. *Nature* **536**, 285-291 (2016).
42. F. Sievers, A. Wilm, D. Dineen, T. J. Gibson, K. Karplus, W. Li, R. Lopez, H. McWilliam, M. Remmert, J. Soding, J. D. Thompson, D. G. Higgins, Fast, scalable generation of high-quality protein multiple sequence alignments using Clustal Omega. *Molecular systems biology* **7**, 539 (2011).
43. J. Soding, A. Biegert, A. N. Lupas, The HHpred interactive server for protein homology detection and structure prediction. *Nucleic acids research* **33**, W244-248 (2005).
44. H. Wu, C. Wang, K. J. Gregory, G. W. Han, H. P. Cho, Y. Xia, C. M. Niswender, V. Katritch, J. Meiler, V. Cherezov, P. J. Conn, R. C. Stevens, Structure of a class C GPCR metabotropic glutamate receptor 1 bound to an allosteric modulator. *Science* **344**, 58-64 (2014).
45. B. Webb, A. Sali, Comparative Protein Structure Modeling Using MODELLER. *Current protocols in bioinformatics / editoral board, Andreas D. Baxevanis ... [et al.]* **47**, 5 6 1-32 (2014).
46. M. A. Nesbit, F. M. Hannan, S. A. Howles, A. A. Reed, T. Cranston, C. E. Thakker, L. Gregory, A. J. Rimmer, N. Rust, U. Graham, P. J. Morrison, S. J. Hunter, M. P. Whyte, G. McVean, D. Buck, R. V. Thakker, Mutations in AP2S1 cause familial hypocalciuric hypercalcemia type 3. *Nature genetics* **45**, 93-97 (2013).
47. F. M. Hannan, S. A. Howles, A. Rogers, T. Cranston, C. M. Gorvin, V. N. Babinsky, A. A. Reed, C. E. Thakker, D. Bockenhauer, R. S. Brown, J. M. Connell, J. Cook, K. Darzy, S. Ehtisham, U. Graham, T. Hulse, S. J. Hunter, L. Izatt, D. Kumar, M. J. McKenna, J. A. McKnight, P. J. Morrison, M. Z. Mughal, D. O'Halloran, S. H. Pearce, M. E. Porteous, M. Rahman, T. Richardson, R. Robinson, I. Scheers, H. Siddique, W. G. Van't Hoff, T. Wang, M. P. Whyte, M. A. Nesbit, R. V. Thakker, Adaptor protein-2 sigma subunit mutations causing familial hypocalciuric hypercalcaemia type 3 (FHH3) demonstrate genotype-phenotype correlations, codon bias and dominant-negative effects. *Human molecular genetics* **24**, 5079-5092 (2015).

48. P. J. Newey, C. M. Gorvin, S. J. Cleland, C. B. Willberg, M. Bridge, M. Azharuddin, R. S. Drummond, P. A. van der Merwe, P. Klenerman, C. Bountra, R. V. Thakker, Mutant prolactin receptor and familial hyperprolactinemia. *N Engl J Med* **369**, 2012-2020 (2013).
49. C. M. Gorvin, F. M. Hannan, S. A. Howles, V. N. Babinsky, S. E. Piret, A. Rogers, A. J. Freidin, M. Stewart, A. Paudyal, T. A. Hough, M. A. Nesbit, S. Wells, T. L. Vincent, S. D. Brown, R. D. Cox, R. V. Thakker, Galpha11 mutation in mice causes hypocalcemia rectifiable by calcilytic therapy. *JCI Insight* **2**, e91103 (2017).
50. Z. Wang, M. Fu, L. Wang, J. Liu, Y. Li, C. Brakebusch, Q. Mei, p21-activated kinase 1 (PAK1) can promote ERK activation in a kinase-independent manner. *The Journal of biological chemistry* **288**, 20093-20099 (2013).
51. T. Bouschet, S. Martin, J. M. Henley, Receptor-activity-modifying proteins are required for forward trafficking of the calcium-sensing receptor to the plasma membrane. *Journal of cell science* **118**, 4709-4720 (2005).
52. C. M. Gorvin, T. Cranston, F. M. Hannan, N. Rust, A. Qureshi, M. A. Nesbit, R. V. Thakker, A G-protein Subunit-alpha11 Loss-of-Function Mutation, Thr54Met, Causes Familial Hypocalciuric Hypercalcemia Type 2 (FHH2). *J Bone Miner Res* **31**, 1200-1206 (2016).
53. M. A. Nesbit, F. M. Hannan, S. A. Howles, V. N. Babinsky, R. A. Head, T. Cranston, N. Rust, M. R. Hobbs, H. Heath, 3rd, R. V. Thakker, Mutations affecting G-protein subunit alpha11 in hypercalcemia and hypocalcemia. *N Engl J Med* **368**, 2476-2486 (2013).
54. V. A. Avlani, W. Ma, H. C. Mun, K. Leach, L. Delbridge, A. Christopoulos, A. D. Conigrave, Calcium-sensing receptor-dependent activation of CREB phosphorylation in HEK293 cells and human parathyroid cells. *American journal of physiology. Endocrinology and metabolism* **304**, E1097-1104 (2013).

Funding: This work was supported by a Wellcome Trust Senior Investigator Award (RVT and CMG); National Institute for Health Research (NIHR) Oxford Biomedical Research Centre Program (RVT); and NIHR Senior Investigator Award (RVT). TM is supported by a long-term fellowship from the Human Frontier Science Program; and VNB was supported by a European Commission Seventh Framework Programme (FP7-264663). The authors would like to thank the NHLBI GO Exome Sequencing Project and its ongoing studies which produced and provided exome variant calls for comparison: the Lung GO Sequencing Project (HL-102923), the WHI Sequencing Project (HL-102924), the Broad GO Sequencing Project (HL-102925), the Seattle GO Sequencing Project (HL-102926) and the Heart GO Sequencing Project (HL-103010). **Author Contributions**: CMG, TM, CS, EYJ, FMH, RVT designed research studies; CMG, VNB, TM, PHN conducted experiments; AJS provided clinical data; ACH provided materials; CMG, VNB, TM, FMH analyzed data; CMG, FMH, RVT wrote the manuscript; and CMG, VNB, AJS, TM, PHN, ACH, EYJ, CS, FMH, RVT reviewed and edited the manuscript.. **Competing interests:** The authors declare that they have no competing interests.

FIGURE LEGENDS

Fig. 1. Identification of an R680G CaSR mutation in a family with autosomal dominant hypocalcemia type 1 (ADH1)

(**A**) Pedigree of family with ADH1. The proband (individual II.3) is indicated by an arrow. (**B**) A heterozygous C-to-G transition at nucleotide c.2038 was identified in the proband and his father by Sanger DNA sequencing and confirmed to cosegregate with hypocalcemia. (**C**) This C-to-G transition changes a CGC codon to GGC and is predicted to result in a missense amino acid substitution from Arg to Gly at position 680 in the CaSR protein. (**D**) Multiple sequence alignment of residues surrounding the Arg^{680} (R) residue encompassing extracellular loop 1 (ECL1) and transmembrane domain 3 (TMD3). The Arg^{680} (R) residue, which is evolutionarily conserved, is located within TMD3, and the mutant Gly^{680} (G) residue is shown in red. Conserved residues are shaded in gray.

Fig. 2. The CaSR R680G mutation does not affect intracellular Ca^{2+} signaling

(**A**) Western blot analysis of HEK293 cells expressing wild-type (WT) or ADH1-associated mutant (R680G and L173F) CaSRs. Calnexin is a loading control. (**B**) Intracellular Ca^{2+} (Ca^{2+}_i) responses to changes in extracellular Ca^{2+} concentration ($[Ca^{2+}]_e$) in cells expressing the indicated wild-type or mutant CaSRs in the absence or presence of the allosteric CaSR inhibitor NPS-2143. Inset shows magnification of the curves between 2-3.5mM $[Ca^{2+}]_e$. Data are shown as the mean±SEM from 4-7 transfections, and EC_{50} values with 95% confidence intervals (CIs) are provided (*F*-test). (**C**) Histogram showing EC_{50} values with 95% CIs for cells expressing wild-type or R680G or L173F mutant CaSRs in the absence or presence of NPS-2143. (**D**) Western blot analysis of cells expressing the indicated wild-type and mutant forms of CaSR and used for assessment of NFAT reporter responses. (**E**) $[Ca^{2+}]_e$-induced NFAT reporter responses of cells expressing wild-type or mutant CaSRs. Responses at each $[Ca^{2+}]_e$ are shown as a fold-change of basal (0.1mM) $[Ca^{2+}]_e$ responses and presented as mean±SEM of 4 transfections. *p<0.05, **p<0.01 ****p<0.0001 using 2-way ANOVA with Tukey's multiple-comparisons tests versus cells expressing wild-type CaSR at each $[Ca^{2+}]_e$.

Fig. 3. The CaSR R680G mutation increases downstream MAPK signaling

(**A**) Western blot analysis showing Ca^{2+}_e-induced phosphorylation of ERK1/2 (pERK1/2) in HEK293 cells expressing wild-type (WT) or ADH1-associated CaSR mutants (R680G or L173F). (**B**) Densitometric analysis of Western blot data in panel A. (**C**) Western blot analysis showing transgenic expression of the indicated forms of CaSR in cells used to assess Ca^{2+}_e-induced phosphorylation of ERK1/2 by AlphaScreen analysis. Calnexin is a loading control. (**D**) Ca^{2+}_e-induced ERK1/2 phosphorylation in CaSR-expressing cells as measured by AlphaScreen analysis, shown as the ratio of phosphorylated ERK1/2 (pERK) to total ERK. (**E**) Western blot analysis showing transgenic expression of the indicated forms of CaSR in cells used to assess Ca^{2+}_e-induced SRE reporter activity. (**F**) Ca^{2+}_e-induced SRE reporter activity in CaSR-expressing cells. (**G**) Western blot analysis showing transgenic expression of CaSR in cells used to assess the effects of NPS-2143 on Ca^{2+}_e-induced SRE responses. (**H**) SRE reporter activity in CaSR-expressing cells in the absence or presence of the allosteric CaSR inhibitor. Data shows mean±SEM values for N=4-20 independent transfections. **p<0.01, ***p<0.001, ****p<0.0001 for $CaSR^{R680G}$ versus $CaSR^{WT}$; $^{\$\$\$}$p<0.001, $^{\$\$\$\$}$p<0.0001 for $CaSR^{L173F}$ versus $CaSR^{WT}$ in panels B, D and F. §§p<0.01, §§§p<0.001 for NPS-2143-treated cells compared to respective untreated cells in panel H. Two-way ANOVA with Tukey's multiple-comparisons test.

Fig. 4. The CaSR R680G mutation does not affect $G_{q/11}$-mediated signaling

(**A**) Western blot analysis of HEK293 cells expressing wild-type (WT) or ADH1-associated CaSR mutants (R680G or L173F). These cells were used for assessment of IP_1 responses. Calnexin is a loading control. (**B**) $Ca^{2+}{}_e$-induced IP_1 fold change in cells expressing the indicated forms of CaSR. (**C**) Western blot analysis of cells used to assess the effect of the $G\alpha_{q/11}$ inhibitors YM-254890 (YM) and UBO-QIC (UBO), on SRE reporter activity. (**D**) $[Ca^{2+}]_e$-induced SRE reporter activity in cells expressing the indicated forms of CaSR in the presence or absence of YM. (**E**) $[Ca^{2+}]_e$-induced SRE reporter in cells expressing the indicated forms of CaSR in the presence or absence of UBO-QIC. Data shows mean±SEM for 8-12 independent transfections. *p<0.05, **p<0.01 ****p<0.0001 for untreated cells expressing $CaSR^{WT}$ versus untreated (black) or YM- or UBO-QIC–treated (blue) cells expressing $CaSR^{R690G}$ in panels D and E. $^{\$}p<0.05$, $^{\$\$}p<0.01$, $^{\$\$\$\$}p<0.0001$ for untreated cells expressing $CaSR^{WT}$ versus untreated (black), or YM- or UBO-QIC–treated (red) cells expressing $CaSR^{L173F}$ in panels B, D and E (2-way ANOVA with Tukey's multiple-comparisons test).

Fig. 5. The CaSR R680G mutation does not affect $G_{i/o}$-mediated signaling

(**A**) Western blot analysis of HEK293 cells expressing wild-type (WT) or ADH1-associated CaSR mutants (R680G or L173F). These cells were used for assessment of cAMP responses. Calnexin is a loading control. (**B**) $Ca^{2+}{}_e$-induced fold change in cAMP abundance in cells expressing the indicated forms of CaSR. (**C**) Histograms showing the cAMP IC_{50} with 95% confidence intervals for cells expressing the indicated forms of CaSR. (**D**) Western blot analysis of cells expressing the indicated forms of CaSR in the presence of pertussis toxin (PTx) or vehicle (Veh). These cells were used to assess effect of PTx on SRE reporter activity. (**E**) Fold change in $[Ca^{2+}]_e$-induced SRE reporter activity in cells expressing the indicated forms of CaSR in the absence or presence of PTx. (**F**) Histograms showing area under the curve (AUC) of SRE reporter responses in vehicle- or PTx-treated cells expressing the indicated forms of CaSR. Data shows mean±SEM for 4-12 independent transfections. *p<0.05, ****p<0.0001 for $CaSR^{R680G}$ compared to $CaSR^{WT}$ in panels E-F. $^{\$}$p<0.05, $^{\$\$\$\$}$p<0.0001 for $CaSR^{L173F}$ compared to $CaSR^{WT}$ in panels B, C, E and F (2-way ANOVA with Tukey's multiple-comparisons test).

Fig. 6. Increased MAPK responses in cells expressing CaSR^{R680G} involve a G-protein–independent, β-arrestin–dependent pathway

(**A-B**) Western blot analysis of HEK293 cells expressing wild-type (WT) or ADH1-associated CaSR mutants (R680G or L173F) and treated with scrambled siRNA (-) or siRNAs targeting (A) β-arrestin1 (βarr1) or (B) β-arrestin2 (βarr2). Calnexin was used as a loading control. (**C-D**) $[Ca^{2+}]_e$-induced SRE reporter responses in cells expressing CaSR^{R680G} and treated with a scrambled siRNA or with siRNAs targeting (C) βarr1or (D) βarr2 or a scrambled siRNA. (**E-F**) $[Ca^{2+}]_e$-induced SRE reporter responses in cells expressing CaSR^{L173F} and treated with siRNAs targeting βarr1 (E) or βarr2 (F) or a scrambled siRNA. The responses of cells treated with siRNAs targeting β-arrestin were compared to the respective cells treated with scrambled siRNA using a 2-way ANOVA with Tukey's multiple-comparisons test. $^{\$}p<0.05$ and $^{\$\$}p<0.0001$ for scrambled vs siRNA for cells expressing wild-type (black) or R680G (blue) CaSR; *p<0.05, **p<0.01, ***p<0.001, ***p<0.0001 for scrambled siRNA treatment of cells expressing wild-type CaSR vs mutant CaSR (blue) and scrambled siRNA treatment of cells expressing wild-type CaSR vs targeted (β-arrestin) siRNA treated mutant CaSR (black). Data is shown as mean±SEM for 8-16 independent transfections.

Fig. 7. The Arg^{680} residue of CaSR forms a salt bridge with either Glu^{767} or Glu^{837}

(**A**) Schematic diagram of a CaSR monomer showing the extracellular bi-lobed venus flytrap domain (VFTD), seven transmembrane domains (TMDs 1-7) with extracellular loops 1–3 (ECL1–3) and intracellular loops 1–3 (ICL1–3), and the cytoplasmic domain. The locations of Arg^{680} in TMD3 (R680, blue), Glu^{767} in ECL2 (E767, red), and Glu^{837} in TMD7 (E837, magenta) are indicated. (**B**) Ribbon diagram showing the transmembrane domains of mGluR1 derived from the published crystal structure (*44*) and a model of the CaSR transmembrane regions based on homology to mGluR1. TMDs 1-7 are numbered; e and i indicate the extracellular and cytoplasmic components of the plasma membrane, respectively. (**C**) Close-up view of the mGluR1 binding pocket for the negative allosteric modulator 4-fluoro-*N*-(4-(6-isopropylamino)pyrimidin-4-yl)thiazol-2-yl)-*N*-methylbenzamide (FITM) (magenta and purple molecule), and (**D**) the corresponding region in the CaSR. Distances between selected atoms are indicated with dashed lines.

Fig. 8. Disruption of the Arg^{680}-Glu^{767} salt bridge leads to increased β-arrestin–mediated MAPK signaling

(**A-B**) Western blot analysis of HEK293 cells expressing wild-type or engineered mutant forms of CaSR (E767R or E837R) and treated with siRNAs targeting (**A**) β-arrestin1 (βarr1) or (**B**) β-arrestin2 (βarr2). (**C-D**) $[Ca^{2+}]_e$-induced SRE reporter responses in cells expressing CaSR^{E767R} or CaSR^{E837R} and treated with a scrambled siRNA or with siRNAs targeting (C) βarr1or (D) βarr2. (**E-F**) Western blot analysis of HEK293 cells expressing wild-type CaSR, E767R CaSR, or a double mutant (dm) form of CaSR incorporating both the R680E and E767R mutations and treated with a scrambled siRNA or siRNA targeting (E) βarr1 or (F) βarr2. These cells were used to assess SRE reporter activity following knockdown of βarr1 or βarr2. (**G-H**) $[Ca^{2+}]_e$-induced SRE reporter responses in cells expressing the double mutant CaSR$^{R680E-E767R}$ and treated with a scrambled siRNA or with siRNAs targeting (G) βarr1or (H) βarr2. Data shows mean±SEM for 8-16 independent transfections. *p<0.05, **p<0.001, ****p<0.0001 for E767R versus WT CaSR in panels C-D; $^{\$}$p<0.05, $^{\$\$}$p<0.01, $^{\$\$\$\$}$p<0.0001 for targeted versus scrambled siRNAs for wild-type (black) or E767R (blue) CaSR in panels C-D; $^{\$\$}$p<0.01, $^{\$\$\$}$p<0.001, $^{\$\$\$\$}$p<0.0001 for a comparison between Glu^{680}-Arg^{767} or wild-type CaSR-expressing cells treated with targeted siRNA and respective cells treated with scrambled siRNA in panels G-H (2-way ANOVA with Tukey's multiple-comparisons).

A

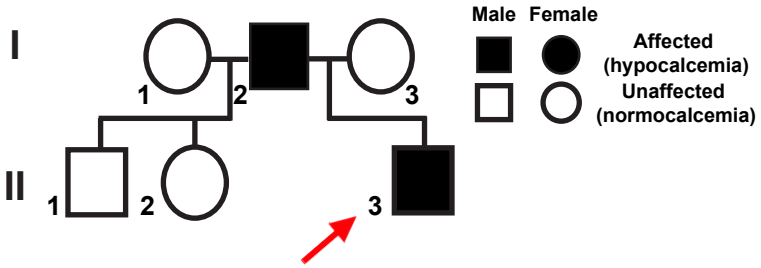

B

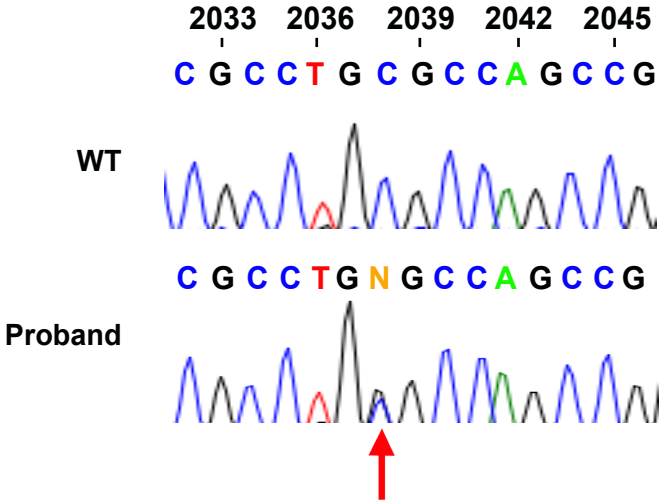

C

Codon	678	679	680	681	682
WT			Arg		
Amino acid	Arg	Leu		Gln	Pro
Mutant			**Gly**		
WT			C		
Nucleotide	CGC	CTG	GC	CAG	CCG
Mutant			**G**		

D

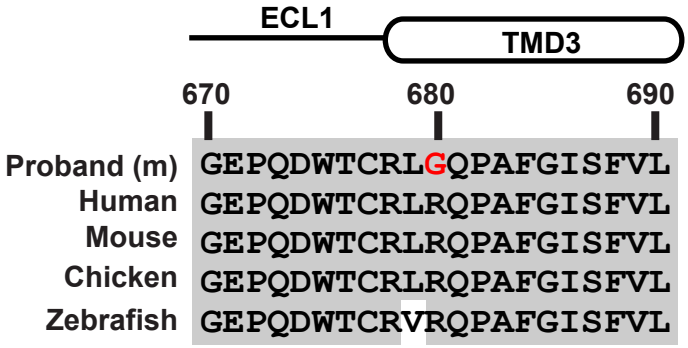

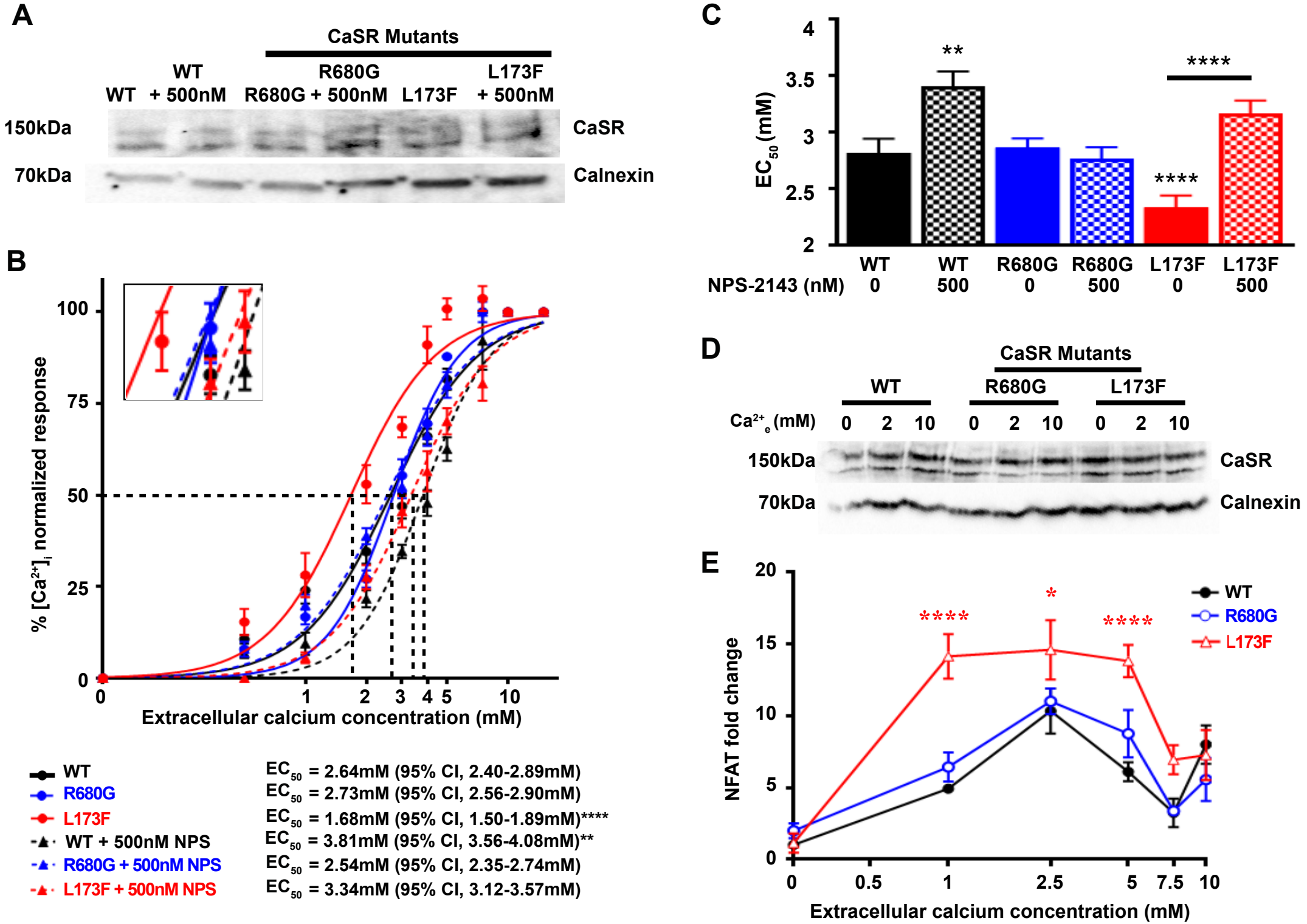
A
CaSR Mutants
WT
WT + 500nM
R680G
R680G + 500nM
L173F
L173F + 500nM
150kDa
CaSR
70kDa
Calnexin
B
% [Ca2+]i normalized response
Extracellular calcium concentration (mM)
WT
R680G
L173F
WT + 500nM NPS
R680G + 500nM NPS
L173F + 500nM NPS
EC50 = 2.64mM (95% CI, 2.40-2.89mM)
EC50 = 2.73mM (95% CI, 2.56-2.90mM)
EC50 = 1.68mM (95% CI, 1.50-1.89mM)****
EC50 = 3.81mM (95% CI, 3.56-4.08mM)**
EC50 = 2.54mM (95% CI, 2.35-2.74mM)
EC50 = 3.34mM (95% CI, 3.12-3.57mM)
C
EC50 (mM)
NPS-2143 (nM)
D
CaSR Mutants
WT
R680G
L173F
Ca2+e (mM)
150kDa
CaSR
70kDa
Calnexin
E
NFAT fold change
Extracellular calcium concentration (mM)
WT
R680G
L173F

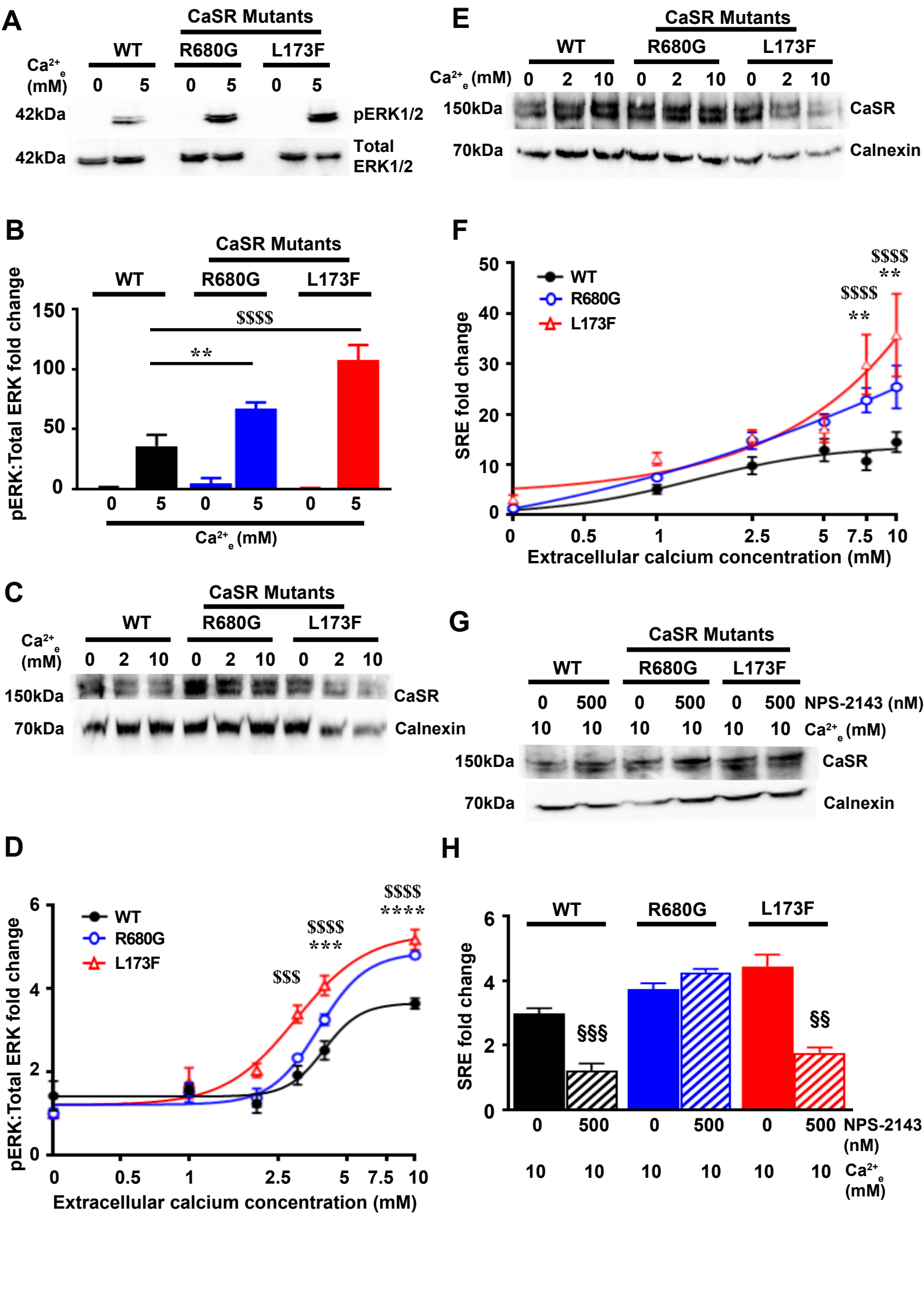
A
CaSR Mutants
WT
R680G
L173F
Ca2+e (mM)
0 5 0 5 0 5
42kDa
pERK1/2
42kDa
Total ERK1/2
B
CaSR Mutants
WT
R680G
L173F
pERK:Total ERK fold change
150
100
50
0
$$$$
**
0 5 0 5 0 5
Ca2+e (mM)
C
CaSR Mutants
WT
R680G
L173F
Ca2+e (mM)
0 2 10 0 2 10 0 2 10
150kDa
CaSR
70kDa
Calnexin
D
WT
R680G
L173F
$$$
$$$$
***
$$$$
****
pERK:Total ERK fold change
6
4
2
0
0 0.5 1 2.5 5 7.5 10
Extracellular calcium concentration (mM)
E
CaSR Mutants
WT
R680G
L173F
Ca2+e (mM)
0 2 10 0 2 10 0 2 10
150kDa
CaSR
70kDa
Calnexin
F
WT
R680G
L173F
$$$$
**
$$$$
**
SRE fold change
50
40
30
20
10
0
0 0.5 1 2.5 5 7.5 10
Extracellular calcium concentration (mM)
G
CaSR Mutants
WT
R680G
L173F
0 500 0 500 0 500 NPS-2143 (nM)
10 10 10 10 10 10 Ca2+e (mM)
150kDa
CaSR
70kDa
Calnexin
H
WT
R680G
L173F
SRE fold change
6
4
2
0
§§§
§§
0 500 0 500 0 500 NPS-2143 (nM)
10 10 10 10 10 10 Ca2+e (mM)

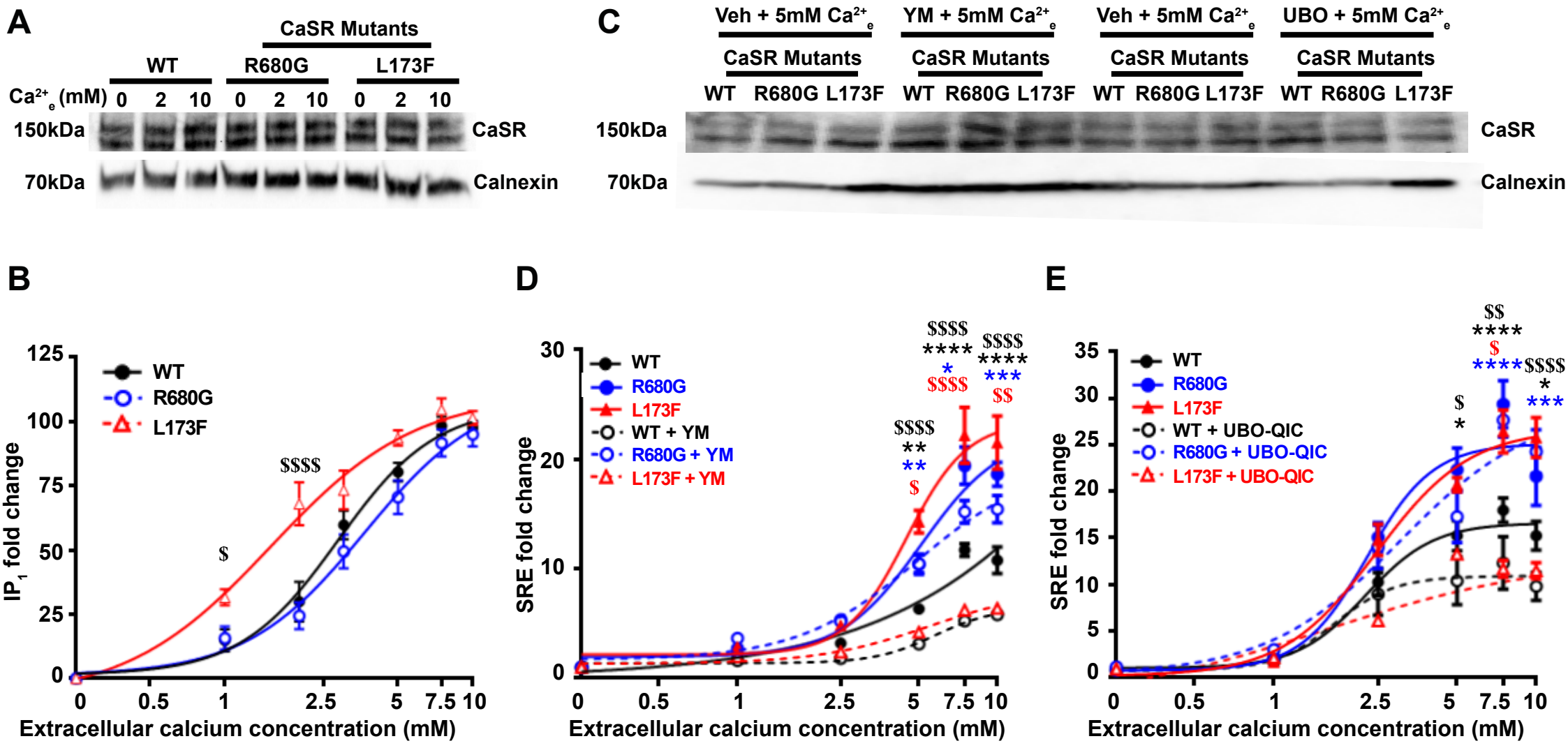
A
CaSR Mutants
WT
R680G
L173F
Ca2+e (mM) 0 2 10 0 2 10 0 2 10
150kDa
CaSR
70kDa
Calnexin
C
Veh + 5mM Ca2+e
YM + 5mM Ca2+e
Veh + 5mM Ca2+e
UBO + 5mM Ca2+e
CaSR Mutants
WT R680G L173F
150kDa
CaSR
70kDa
Calnexin
B
IP1 fold change
WT
R680G
L173F
Extracellular calcium concentration (mM)
D
SRE fold change
WT
R680G
L173F
WT + YM
R680G + YM
L173F + YM
Extracellular calcium concentration (mM)
E
SRE fold change
WT
R680G
L173F
WT + UBO-QIC
R680G + UBO-QIC
L173F + UBO-QIC
Extracellular calcium concentration (mM)

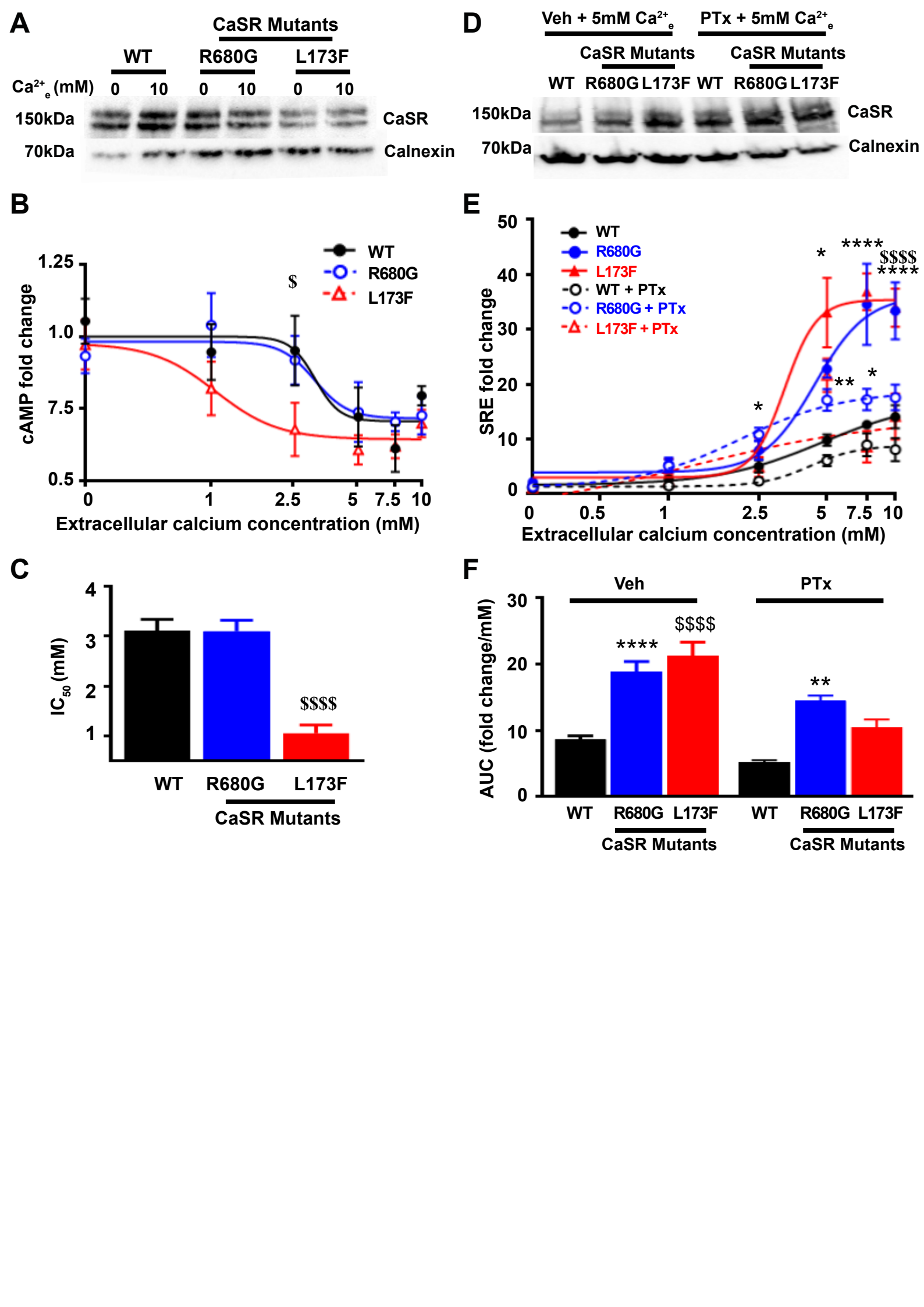
A
CaSR Mutants
WT
R680G
L173F
Ca2+e (mM)
0
10
0
10
0
10
150kDa
CaSR
70kDa
Calnexin
D
Veh + 5mM Ca2+e
PTx + 5mM Ca2+e
CaSR Mutants
CaSR Mutants
WT R680G L173F WT R680G L173F
150kDa
CaSR
70kDa
Calnexin
B
WT
R680G
L173F
$
cAMP fold change
1.25
1.0
7.5
0.5
0
1
2.5
5
7.5
10
Extracellular calcium concentration (mM)
E
WT
R680G
L173F
WT + PTx
R680G + PTx
L173F + PTx
SRE fold change
50
40
30
20
10
0
0
0.5
1
2.5
5
7.5
10
Extracellular calcium concentration (mM)
*
****
$$$$
****
**
*
*
C
IC50 (mM)
4
3
2
1
$$$$
WT
R680G
L173F
CaSR Mutants
F
Veh
PTx
AUC (fold change/mM)
30
20
10
0
****
$$$$
**
WT
R680G
L173F
WT
R680G
L173F
CaSR Mutants
CaSR Mutants

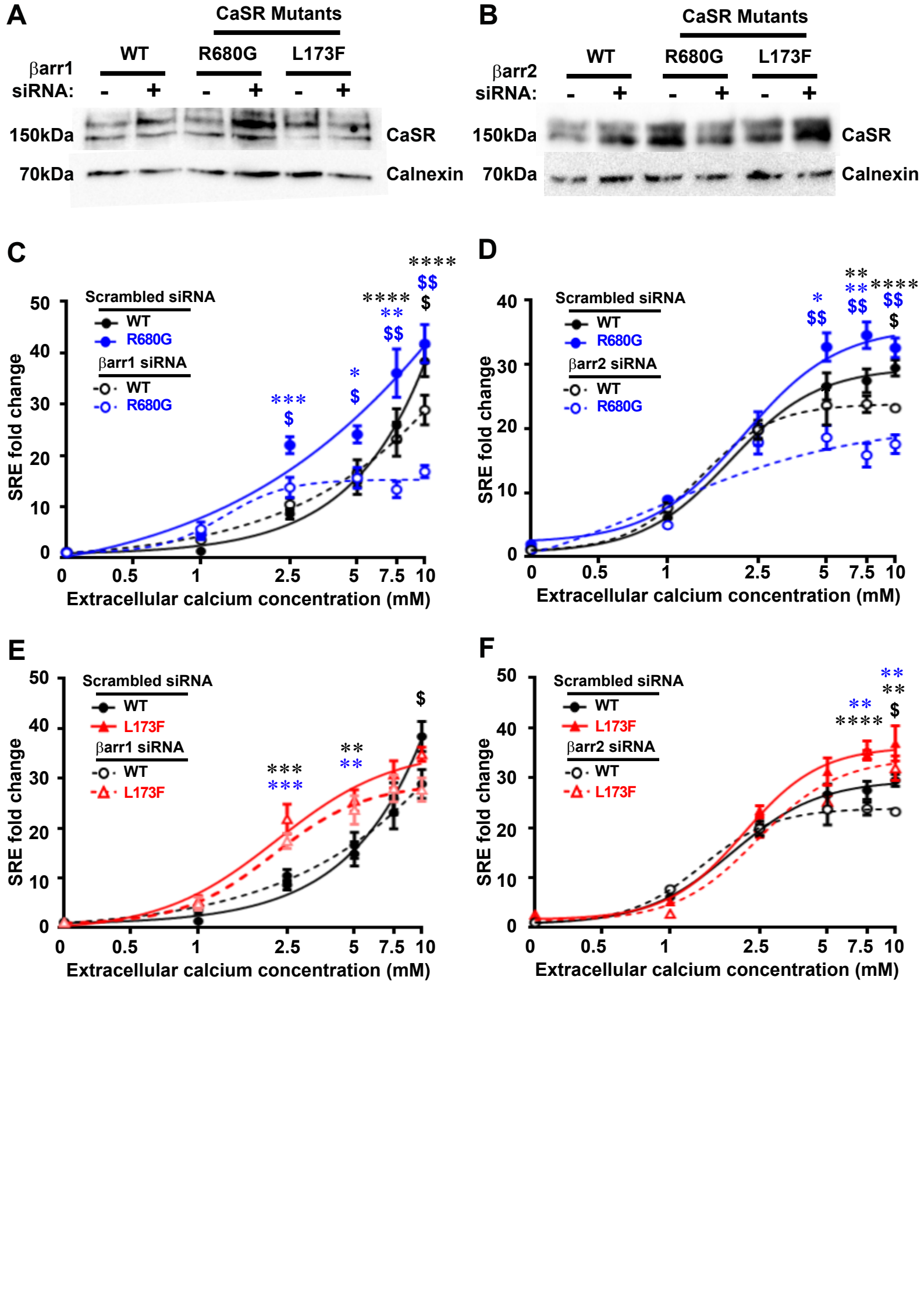
A
CaSR Mutants
WT
R680G
L173F
βarr1 siRNA:
- + - + - +
150kDa
CaSR
70kDa
Calnexin
B
CaSR Mutants
WT
R680G
L173F
βarr2 siRNA:
- + - + - +
150kDa
CaSR
70kDa
Calnexin
C
Scrambled siRNA
WT
R680G
βarr1 siRNA
WT
R680G
SRE fold change
Extracellular calcium concentration (mM)
D
Scrambled siRNA
WT
R680G
βarr2 siRNA
WT
R680G
SRE fold change
Extracellular calcium concentration (mM)
E
Scrambled siRNA
WT
L173F
βarr1 siRNA
WT
L173F
SRE fold change
Extracellular calcium concentration (mM)
F
Scrambled siRNA
WT
L173F
βarr2 siRNA
WT
L173F
SRE fold change
Extracellular calcium concentration (mM)

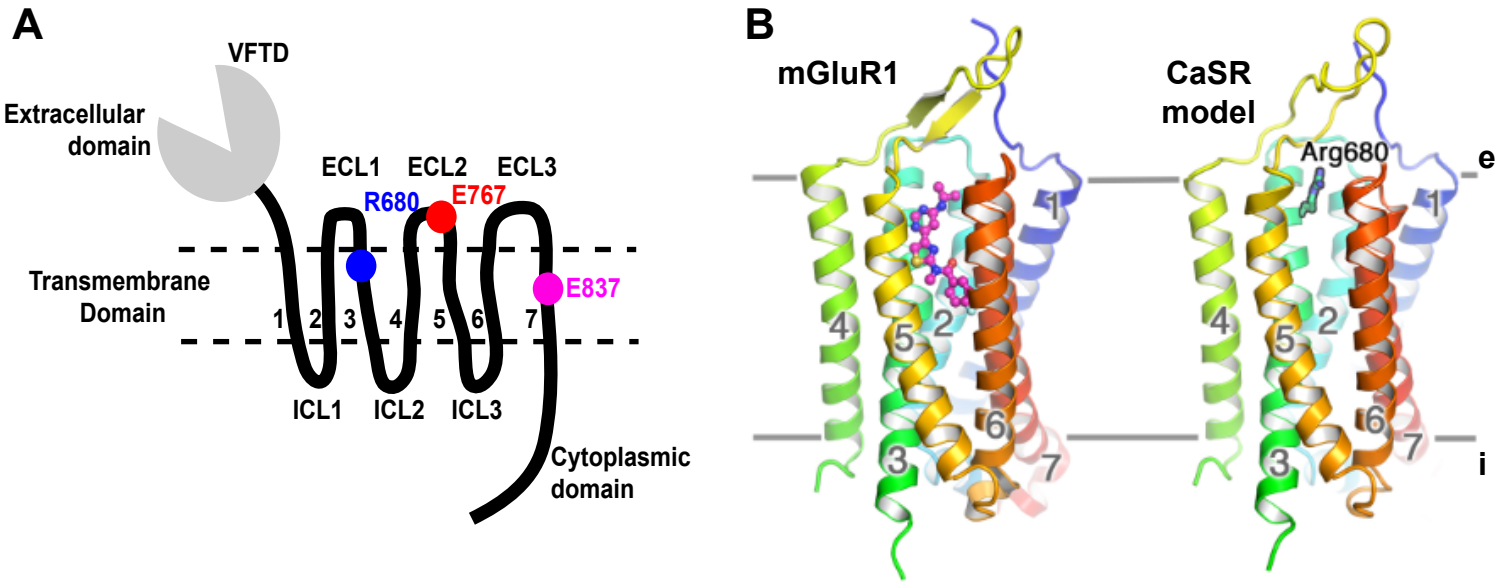
A
VFTD
Extracellular domain
ECL1
ECL2
ECL3
R680
E767
E837
Transmembrane Domain
1
2
3
4
5
6
7
ICL1
ICL2
ICL3
Cytoplasmic domain
B
mGluR1
CaSR model
Arg680
e
i
C
mGluR1
Gln660
4.1 Å
7.2 Å
Thr748
Thr815
FITM
D
CaSR
Arg680
3.3 Å
Glu767
5.7 Å
Glu837

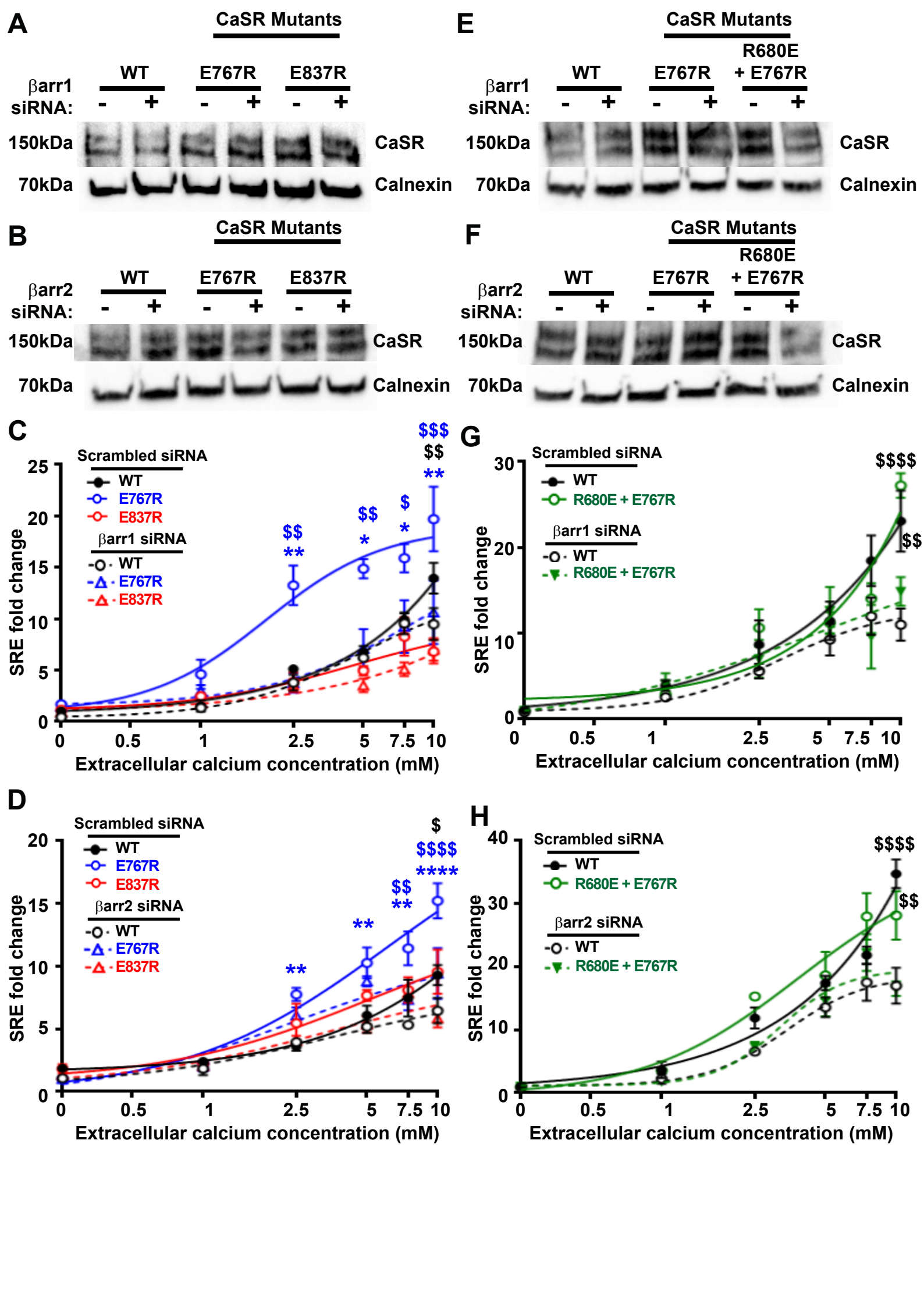
A
CaSR Mutants
WT
E767R
E837R
βarr1 siRNA:
- + - + - +
150kDa
CaSR
70kDa
Calnexin
E
CaSR Mutants
WT
E767R
R680E + E767R
βarr1 siRNA:
- + - + - +
150kDa
CaSR
70kDa
Calnexin
B
CaSR Mutants
WT
E767R
E837R
βarr2 siRNA:
- + - + - +
150kDa
CaSR
70kDa
Calnexin
F
CaSR Mutants
WT
E767R
R680E + E767R
βarr2 siRNA:
- + - + - +
150kDa
CaSR
70kDa
Calnexin
C
Scrambled siRNA
WT
E767R
E837R
βarr1 siRNA
WT
E767R
E837R
SRE fold change
Extracellular calcium concentration (mM)
0 0.5 1 2.5 5 7.5 10
0 5 10 15 20 25
$$$
$$
**
$$
*
$
*
$$
**
G
Scrambled siRNA
WT
R680E + E767R
βarr1 siRNA
WT
R680E + E767R
SRE fold change
Extracellular calcium concentration (mM)
0 0.5 1 2.5 5 7.5 10
0 10 20 30
$$$$
$$
D
Scrambled siRNA
WT
E767R
E837R
βarr2 siRNA
WT
E767R
E837R
SRE fold change
Extracellular calcium concentration (mM)
0 0.5 1 2.5 5 7.5 10
0 5 10 15 20
$
$$$$
****
$$
**
**
**
H
Scrambled siRNA
WT
R680E + E767R
βarr2 siRNA
WT
R680E + E767R
SRE fold change
Extracellular calcium concentration (mM)
0 0.5 1 2.5 5 7.5 10
0 10 20 30 40
$$$$
$$